Toward a Surface Soil Moisture Product at High Spatiotemporal Resolution: Temporally Interpolated, Spatially Disaggregated SMOS Data

Yoann Malbéteau, Olivier Merlin, G. Balsamo, S. Er-Raki, S. Khabba, J. P Walker, Lionel Jarlan

Towards a surface soil moisture product at high spatio-temporal resolution: temporally-interpolated spatially-disaggregated SMOS data

Y. Malbéteau*

CESBIO, Université de Toulouse, CNES/CNRS/IRD/UPS, Toulouse, France

O. Merlin

CESBIO, Université de Toulouse, CNES/CNRS/IRD/UPS, Toulouse, France

G. Balsamo

European Centre for Medium-Range Weather Forecasts, Reading, United Kingdom

S. Er-Raki

Faculté des Sciences et Techniques, Université Cadi Ayyad (UCAM), Marrakech, Morocco

S. Khabba

Faculté des Sciences Semlalia, Université Cadi Ayyad (UCAM), Marrakech, Morocco

J.P. Walker

Department of Civil Engineering, Monash University, Melbourne, Australia

L. Jarlan

CESBIO, Université de Toulouse, CNES/CNRS/IRD/UPS, Toulouse, France

* *Corresponding author address:* CESBIO, Université de Toulouse, CNES/CNRS/IRD/UPS, Toulouse, France

E-mail: yoann.malbeteau@cesbio.cnes.fr

ABSTRACT

High spatial and temporal resolution surface soil moisture is required for most hydrological and agricultural applications. The recently developed DisPATCh (DISaggregation based on Physical And Theoretical scale Change) algorithm provides 1-km resolution surface soil moisture by downscaling the 40-km SMOS (Soil moisture Ocean Salinity) soil moisture using MODIS (MODerate-resolution Imaging Spectroradiometer) data. However, the temporal resolution of DisPATCh data is constrained by the temporal resolution of SMOS (a global coverage every 3 days) and further limited by gaps in MODIS images due to cloud cover. This paper proposes an approach to overcome these limitations based on the assimilation of the 1-km resolution DisPATCh data into a simple dynamic soil model forced by (inaccurate) precipitation data. The performance of the approach was assessed using ground measurements of surface soil moisture in the Yanco area in Australia and the Tensift-Haouz region in Morocco during 2014. It was found that the analyzed daily 1-km resolution surface soil moisture compared slightly better to *in situ* data for all sites than the original disaggregated soil moisture products. Over the entire year, assimilation increased the correlation coefficient between estimated soil moisture and ground measurement from 0.53 to 0.70, whereas the mean ubRMSE slightly decreased from 0.07 m^3 m^{-3} to 0.06 m^3 m^{-3} compared to the open-loop force-restore model. The proposed assimilation scheme has significant potential for large scale applications over semi arid areas, since the method is based on data available at global scale together with a parsimonious land surface model.

1. Introduction

Soil moisture is an important variable of the terrestrial hydrosphere. Whereas precipitation provides the amount of available water at the surface, soil moisture impacts the partitioning of rainfall into runoff, evaporation and infiltration. Moreover, soil moisture is highly variable in space and time, as a result of (1) the alternation between wetting and drying events, and (2) the heterogeneity in land cover, topography and soil properties. An accurate and continuous description of soil moisture in space and time is therefore critical for understanding the continental water cycle and for achieving efficient and sustainable water management (Entekhabi 1995; Gao et al. 2014; Rodriguez-Iturbe 2000).

Satellite remote sensing is often the most practical and effective method to observe the land surface soil moisture over large geographical areas. The recent Soil Moisture and Ocean Salinity (SMOS) mission, launched in 2009, operates at L-band (the optimal microwave band to estimate soil moisture (Kerr 2007; Njoku and Entekhabi 1996)) and provides near-surface soil moisture (SSM) with a resolution of about 40 km (Kerr et al. 2012). This mission has been complemented by the SMAP (Soil Moisture Active Passive) satellite mission launched in 2015; ensuring the continuity of L-band passive microwave data for global SSM monitoring (Entekhabi et al. 2010b). Recent studies, based on the temporal stability of soil moisture (Vachaud et al. 1985), have shown that even coarse scale satellite soil moisture can add a benefit in hydrological modeling (Pauwels et al. 2001; Draper et al. 2011; Brocca et al. 2012; Alvarez-Garreton et al. 2015; Chen et al. 2014; Massari et al. 2015; Lievens et al. 2015b). Nevertheless, the current spatial resolution of microwave radiometers is too coarse for most hydrological and agricultural applications. Therefore, downscaling methodologies have been developed to improve the spatial resolution of

passive microwave-derived SSM data (Das et al. 2014; Fang et al. 2013; Kim and Hogue 2012; Merlin et al. 2008a; Piles et al. 2011; Sánchez-Ruiz et al. 2014; Srivastava et al. 2013). For example, DisPATCh (DISaggregation based on Physical And Theoretical scale Change) estimates the SSM variability within a 40 km resolution SMOS pixel at 1 km resolution using MODIS (MODerate-resolution Imaging Spectroradiometer) data (Merlin et al. 2012, 2013). However, the temporal resolution of DisPATCh data based on SMOS and MODIS data is limited by 1) gaps in MODIS images due to cloud cover, and 2) the 2-3 day temporal resolution of global SMOS coverage (Djamai et al. 2016).

A land surface model (LSM) forced by uncertain meteorological inputs and constrained with discontinuous disaggregated soil moisture through data assimilation could both address the issue of discontinuity in the soil moisture products and as well as improve the SSM estimate. Several studies have been undertaken to assimilate the observed satellite brightness temperature directly (Crow and Wood 2003; Dumedah et al. 2011; Margulis et al. 2002; Reichle et al. 2007; Lievens et al. 2015a, 2017) and/or the satellite SSM retrieval (Reichle et al. 2008; Draper et al. 2011; Brocca et al. 2012; Dumedah and Walker 2014; Ridler et al. 2014; Kumar et al. 2014; Wanders et al. 2014; Lievens et al. 2015b; Leroux et al. 2016) into LSMs. Others studies have assimilated coarse scale SSM into a fine land surface models to produce fine model predictions and consistently improve soil moisture and other land surface variables (Reichle et al. 2001b, 2010; Parada and Liang 2004; Pan et al. 2009a,b; De Lannoy et al. 2010, 2012; De Lannoy and Reichle 2016; Sahoo et al. 2013; Lievens et al. 2016, 2017). These approaches are based on spatial error correlations that are modeled within the assimilation system. Moreover, Djamai et al. (2016) estimated SSM at 1 km resolution during cloudy days by combining DisPATCh data and the Canadian Land Surface Scheme (CLASS), forced by a 30 km atmospheric re-analysis. However,

the SSM DisPATCh estimates were not improved by the combination of DisPATCh and CLASS when compared to *in situ* measurements of the SMAP Validation Experiments data set in 2012 over Winnipeg in Canada. In a similar context, Dumedah et al. (2015) assimilated DisPATCh data into the Joint UK Land and Environment Simulator (JULES) to estimate root zone soil moisture over the Yanco area in Australia. The assimilation of DisPATCh data into the JULES model had a limited positive impact on the SSM estimation accuracy compared to DisPATCh and open-loop JULES simulation.

These results demonstrate that data assimilation remains one of the most promising approaches to link satellite based SSM with LSMs, while accounting for uncertainties in the observation data and the simulated output from the model (Calvet et al. 1998; Entekhabi et al. 1994; Jackson et al. 1981; Reichle et al. 2001a; Sabater et al. 2007). However, assimilation strategies still need to be improved. Two aspects should be addressed when assimilating downscaled SSM data into a LSM: 1) the number of state variables in the LSM should be consistent with the available observations in order to eliminate equifinality (Beven 1989; Franks et al. 1997), and 2) the accuracy in forcing data at the application scale. Most of surface models developed since the 80s (Sellers et al. 1986; Noilhan and Planton 1989) have a large number of variables which cannot be directly measured at the model application scale (Demaria et al. 2007; Franks et al. 1997). As over-parameterization is the main limitation for implementation of such complex models in an operational context, there is a need to develop simplified modeling approaches that are forced by available remote sensing and meteorological data (Allen et al. 1998). A number of studies have shown the potential of this approach (Albergel et al. 2008; Ceballos et al. 2005; Pellarin et al. 2006; Wagner et al. 1999) for representing components of the surface water budget. One of the main issues is that large-scale data sets of meteorological variables are currently unavailable at 1 km (or higher)

spatial resolution. Nevertheless, a disaggregation/assimilation coupling scheme is potentially capable of compensating errors in atmospheric (mainly precipitation) forcing data available at a coarse scale only (Merlin et al. 2006).

Within this context, the objective of this study was to develop a new methodology based on an assimilation scheme for interpolating DisPATCh SSM in a sub-optimal manner using global (meteorological and soil map) datasets. Since DisPATCh is a physically-based method to provide natively SSM at 1 km resolution using 1 km resolution MODIS data, the native resolution of the DisPATCh SSM products developed is 1 km resolution. The approach was tested using ground measurements of soil moisture and precipitation over two semi arid sites: 1) the Yanco area in the Murrumbidgee river catchment, Australia and 2) the Tensift-Haouz basin located in central Morocco.

2. Sites description

a. Yanco: Murrumbidgee catchment (Australia)

The Murrumbidgee catchment, located in southeastern of Australia, covers about 82,000 km^2 (34°S to 37°S, 143°E to 150°E) and is a part of the Murray Darling basin. The Yanco study site is a 55 km x 55 km area located in the center of the Murrumbidgee western plains where the topography is flat, with very few geological outcropping. The soil texture is predominantly sandy loam. The climate is semi-arid, with an average annual precipitation of about 300 mm while evaporative demand is about 1,200 mm per year, according to the reference evapotranspiration (ET0), derived from the Food and Agriculture Organization (FAO) Penman Monteith equation (Allen et al. 1998). The land use in the west of the site comprises irrigation, while elsewhere land

use is composed of rain-fed crops and native pasture with scattered trees.

The Yanco region has been intensively monitored for remote sensing studies since 2001 (Smith et al. 2012). This area has been selected as a core site for the calibration/validation of the SMOS (Peischl et al. 2012), SMAP (Panciera et al. 2014), and GCOM-W1 (Mladenova et al. 2011) missions, and has also been the focus of field experiments dedicated to algorithm development studies for the SMOS and SMAP missions: National Airborne Field Experiment 2006 (NAFE06; Merlin et al. (2008b)); Australian Airborne Cal/Val Experiments for SMOS (AACES-1, -2; Peischl et al. (2012)) and Soil Moisture Active Passive Experiments (SMAPex-1, -2, -3; Panciera et al. (2014)). To assess the ERA-interim precipitation product, OzNet ground based precipitation measurements using tipping bucket rain gauges were used (Smith et al. 2012). These data are available on the World Wide Web at http://www.oznet.org.au/. Seven sites presenting the best data quality and continuity were selected for this study (Yanco 1, 2, 8, 9, 10, 12 and 13). Table 1 displays the site characteristics, and their locations are shown in Fig. 1. These sites are representative of the 3 main land uses of the region (Fig. 1): irrigated crops (Yanco 9), rain-fed crops (Yanco 1 and 11; typically wheat and fallow), and grazing (Yanco 2, 8, 10, 13; typically perennial grass type vegetation).

Fig. 1

b. Tensift-Haouz basin (Morocco)

The Tensift-Haouz basin covers about 24,000 km^2 (30.75°N 32.40°N and 7.05°E to 9.9°W) around the city of Marrakech, in central Morocco (Fig. 2). The climate is semi-arid, typically Mediterranean, with an average annual precipitation of about 250 mm (Chehbouni et al. 2008) concentrated between November and April over the Haouz plain, where the study site is located.

Evaporative demand is about 1,600 mm per year.

In the Tensift-Haouz basin, the Sidi Rahal monitoring station was installed on a rain-fed wheat field (Fig. 2) in December 2013, in the framework of the Joint International Laboratory TREMA (a French acronym for Remote Sensing and Water Resources in the Semi-arid Mediterranean; http://trema.ucam.ac.ma; Jarlan et al. (2015)). It is equipped with micro-meteorological instruments to estimate latent and sensible heat fluxes at the soil-vegetation-atmosphere interface, and probes for the measurements of soil water content at different depths. The automatic meteorological station installed in the vicinity was equipped with sensors for the measurement of rainfall, global radiation, temperature, relative humidity, and wind speed at a half-hourly time step. The soil texture is predominantly loams. Information about the monitoring stations is provided in Table 1 and Fig. 2.

Fig. 2 and Table 1

3. Materials and method

a. Globally available data

1) SMOS SOIL MOISTURE DATA

The SMOS level 3 one day global SSM (MIR_CLF31A\D, version 7.72 in reprocessing mode RE04) product is used in this study as input to DisPATCh algorithm and assimilation scheme. These products are presented in NetCDF format on the EASE grid, with a grid spacing of $\backsim$25 x 25 km in cylindrical projection. Note that L3 data is a 25 km grid representation of the 40 km data. Details on the processing algorithms can be found in the Algorithm Theoretical Baseline

Document (Jacquette et al. 2013) and in the Level 3 data product description (Kerr et al. 2014). For comparison purpose, the assimilation scheme was applied at 1 km resolution using the non-disaggregated (25 km) SMOS L3 data by oversampling the 25-km product.

2) DisPATCh soil moisture data

DisPATCh provided 1 km resolution SSM data from 40 km SMOS SSM and 1 km MODIS LST (Land Surface Temperature), MODIS NDVI (Normalized Difference Vegetation Index) and GTOPO30 DEM (Digital Elevation Model) data. MODIS-derived soil temperature was used to estimate Soil Evaporative Efficiency (SEE), which is known to be relatively constant during the day on clear sky conditions (Merlin et al. 2012). MODIS-derived 1 km resolution SEE was finally used as a proxy for SSM variability within the low-resolution pixel using a first-order series expansion around the SMOS observation. The disaggregated SSM products are expressed in $m^3\ m^{-3}$. The current version of the DisPATCh methodology is fully described in Molero et al. (2016). Note that only ascending SMOS overpass (6 am) was used in this paper.

The DisPATCh product was derived from the average of an output ensemble for each SMOS overpass time. This output ensemble was obtained by applying DisPATCh to 1) four SMOS re-sampling grids by taking advantage of the Level 3 SMOS data oversampling, 2) three MODIS overpass dates by taking into account the MODIS data collected within plus or minus one day around the SMOS overpass, and 3) two daily MODIS observations aboard Terra and Aqua. The number of elements used to compute this average (a maximum of 24 elements per SMOS overpass) is called the DisPATCh count. Note that the DisPATCh count is often smaller than 24 due to gaps in MODIS data associated with cloud cover and/or limited overlap with the SMOS swath. The error of the DisPATCh product is taken as the standard deviation from the output

ensemble computing. This error accounts for the downscaling and retrieval errors (more details in Merlin et al. (2012); Malbéteau et al. (2016)).

DisPATCh outputs have been validated mostly in semi-arid conditions where SEE is well constrained by the SSM: the Murrumbidgee catchment in Australia (Bandara et al. 2015; Malbéteau et al. 2016; Molero et al. 2016), the Little Washita watershed in Oklahoma, Walnut Gulch in Arizona over USA (Molero et al. 2016), the Tensift-Haouz basin in central Morocco (Merlin et al. 2015) and the Lleida area in Spain (Escorihuela and Quintana-Seguí 2016; Merlin et al. 2013).

3) VEGETATION INDEX

In order to estimate evapotranspiration, the vegetation cover (fv) was derived from the 1 km resolution MODIS NDVI data. The NDVI dataset was extracted from the version-5 MODIS/ Terra vegetation indices 16-day Level-3 global 1-km grid product (MOD13A2). Fractional fv was computed using the linear relationship between NDVI of the fully-covered vegetation and NDVI of the bare soil proposed by Gutman and Ignatov (1998).

4) METEOROLOGICAL DATASET

The ECMWFs (European Centre for Medium-Range Weather Forecasts) Interim re-analysis product (ERA-interim; Dee et al. (2011)) was used for meteorological (relative humidity, air temperature, wind speed, pressure, shortwave and longwave radiations and precipitation) forcing. ERA-Interim is produced at the highest resolution of about 0.125° with a 3-hourly time step covering the period from January 1979 to present, with product updates at approximately 1 month behind real-time. This study used the ERA-interim datasets provided daily at 0.125° spatial resolution. Note that the product is generated at a much coarser resolution (a spectral

T255 horizontal resolution, which corresponds to approximately 79 km spacing grid) and then mapped to 0.125°. The ERA-Interim atmospheric re-analysis is built upon a consistent assimilation of an extensive set of observations distributed worldwide from satellite remote sensing, *in situ* measurements, and radio-sounding. ERA-Interim data sets are free of charge and available via: www.ecmwf.int/en/research/climate-reanalysis/era-interim. The environmental parameters simulated by ERA-Interim have been widely validated by *in situ* and remote sensing observations at different spatio-temporal scales (Balsamo et al. 2015; Bao and Zhang 2013; Boisvert et al. 2015; Mooney et al. 2011; Su et al. 2013; Szczypta et al. 2011; Wang and Zeng 2012). Several studies (Belo-Pereira et al. 2011; Pfeifroth et al. 2013; Szczypta et al. 2011; Zhang et al. 2013) have reported an overestimation of ECMWF precipitation data, but Balsamo et al. (2010) have shown that the original ERA-Interim products have reasonable skill for land applications at time scales from daily to annual over the conterminous US. The total annual amount and daily distribution of ECMWF precipitation is compared to meteorological stations in this study for the two test sites.

5) GLOBAL SOIL TEXTURE

The relative amounts of bound and free water are influenced by the soil texture (sand, clay and silt fractions) and bulk density. The map used for this study was a 0.01° resolution combination of the soil maps (Kim 2013) from 1) FAO (Food and Agriculture Organization) and 2) HWSD (Harmonized World Soil Database), and the regional datasets 1) STATSGO (State Soil GeographicUS), 2) NSDC (National Soil Database Canada), and 3) ASRIS (Australian Soil Resources Information System). Note that this soil texture map is used by both SMOS (Kerr et al. 2012) and SMAP (Entekhabi et al. 2010b) level 2 SSM retrieval algorithms.

b. Land surface model (LSM)

In an effort to reduce as much as possible the number of model parameters, while attempting to preserve the representation of the physics which controls the SSM dynamics, the LSM used in this study was based on the force-restore method developed by Deardorff (1977). This scheme is used in many LSMs including ISBA (Interactions between Soil Biosphere Atmosphere; Noilhan and Planton (1989)). The force-restore method appears to be a good tradeoff between realism (physics) and complexity (number of parameters) for calibration over large areas. In this semi-physical model, the dynamics of soil moisture is described within two layers: the SSM (noted Θ_1) and the root zone soil moisture (noted Θ_2). In this study, only the SSM dynamics were simulated with the root-zone soil moisture taken as a buffer variable to minimize possible biases between DisPATCh SSM and the force restore prediction for compensating errors in meteorological (mainly precipitation and irrigation) forcing data. The equation for SSM is:

$$\frac{\partial \Theta_1}{\partial t} = \frac{C_1}{\rho_w d_1}(P - E_g) - \frac{C_2}{\tau}(\Theta_1 - \Theta_{eq}), \tag{1}$$

with Θ_{eq} the equilibrium soil moisture, P the ERA-interim precipitation reaching the soil surface, E_g the evaporation at the soil surface, ρ_w the density of liquid water, τ the time constant taken as one day and d_1 an arbitrary normalization depth of 10 cm. C_1 and C_2 are empirical parameters named force and restore coefficients, respectively representing the process of mass exchange between the soil and the atmosphere, and the surface and the root-zone layer, respectively. The force and restore coefficients C_1 and C_2 are dimensionless and highly dependent upon both the soil moisture content and the soil texture. Note that coefficients C_1 and C_2 are spatially distributed based on Noilhan and Mahfouf (1996) and vary over time. They were calibrated against a multi-layer soil moisture model (Noilhan and Mahfouf 1996) such that

$$C_1 = C_{1sat}\left(\frac{\Theta_{sat}}{\Theta_1}\right)^{(\frac{\beta}{2}+1)}, \tag{2}$$

$$C_2 = C_{2ref}\left(\frac{\Theta_2}{\Theta_{sat}-\Theta_2+\Theta_l}\right), \tag{3}$$

with Θ_{sat} being the saturated soil moisture for a given texture, β the slope of the retention curve, C_{1sat} and C_{1ref} hydraulic parameters and Θ_l a small numerical value equal to 0.001. Each parameter was estimated from clay/sand fractions and default empirical parameters (equations are detailed in Noilhan and Mahfouf (1996)). E_g in equation 1 is expressed as in Allen (2000) and Allen et al. (2005) by

$$E_g = ET_0 \times K_e, \tag{4}$$

with ET_0 being the reference evapotranspiration estimated according to the FAO Penman-Monteith equation (Allen et al. 1998) and the ERA-interim meteorological forcing data (relative humidity, air temperature, wind speed, pressure, shortwave and longwave radiations). K_e the soil evaporation coefficient computed from

$$K_e = (1-f_v)K_r, \tag{5}$$

with K_r the soil evaporation reduction coefficient derived from the SSM. Soil evaporation from the exposed soil was assumed to take place in two stages: an energy limiting stage and a falling rate stage. After rain, evaporation was only determined by the energy available for evaporation, thus K_r was set to 1; then when the soil surface dried out, K_r decreased linearly and evaporation was reduced. K_r was equal to zero when no significant water was left for evaporation, being when

SSM was smaller than $\frac{1}{2}\Theta_{wp}$ (where Θ_{wp} was the soil moisture at wilting point) as reported by Allen et al. (1998).

c. Assimilation scheme: A combined 2D variational and sequential approach

The purpose of assimilating DisPATCh data into a LSM was to combine the downscaled snapshots of DisPATCh SSM with the continuous LSM predictions, in order to obtain the best estimate of the SSM at 1 km every day. The simplified two-dimensional variational (2D VAR) method developed by Balsamo et al. (2004) to analyze the root-zone soil moisture (as a buffer variable) was combined to a simplified Kalman filter approach to update the SSM state. The relation between surface and root-zone soil moisture is not physically based with the force-restore scheme. For that reason a linear variational algorithm may not be well suited for updating surface soil moisture by contrast with the root-zone. Moreover, the sequential approach is able to update the potentially rapid changes related to irrigation that are not represented by the LSM but are observed in DisPATCh data. Thus, the two-scheme procedure has the advantage to consider the two temporal dynamics, being (rapid) surface and (slow) root-zone soil moisture.

The 2D VAR method was initially designed to analyze the root zone soil moisture using 2 m air temperature and humidity observations (Balsamo et al. 2004). It has been adapted by Sabater et al. (2007) to analyze the root zone soil moisture from SSM observations, and to the analysis of both above ground biomass and root zone soil moisture by Sabater et al. (2008). The simplified 2D VAR has also been applied to the analysis of above-ground biomass from satellite-derived leaf area index products over West Africa (Jarlan et al. 2008). In the present study, Θ_2 was taken as a buffer variable without any dynamic equation. Stated differently, this variable was left free to adjust the model prediction to DisPATCh SSM through the simplified 2DVAR approach. This first

step of the assimilation algorithm was necessary to represent SSM dynamics with consistency to the restore parameter. The analyzed state is given by:

$$\Theta^a = \Theta^b + K(y - H\Theta^b), \tag{6}$$

where the superscripts a and b indicate the analysis and background, respectively; y is the DisPATCh SSM and $\mathbf{H}$ is the observation operator that allows the projection of the state vector in the observation space. In the 2D VAR approach, $\mathbf{H}$ is computed from a one side finite difference, while $\mathbf{H}$ is equal to 1 in the sequential approach. The SSM update step is close to that of the Kalman filter, but the propagation of the background error matrix was avoided here for simplicity purpose. $\mathbf{K}$ is called the gain and is calculated as:

$$\mathbf{K} = \mathbf{B}\mathbf{H}^T(\mathbf{H}\mathbf{B}\mathbf{H}^T + \mathbf{R})^{-1}, \tag{7}$$

where $\mathbf{B}$ and $\mathbf{R}$ are the covariance matrices of the background and SSM observations errors, respectively. $\mathbf{R}$ is scalar values equal to σ_{obs} (DisPATCh error). $\mathbf{B}$ is calculated as

$$\mathbf{B} = \begin{pmatrix} \sigma_{\Theta_2} & 0 \\ 0 & \sigma_{\Theta_1} \end{pmatrix} \tag{8}$$

with σ_{Θ_1} is Θ_1 background error and σ_{Θ_2} is Θ_2 background error.

Considering a 1-day assimilation window, $\mathbf{H}$ equals to :

$$\mathbf{H} = \begin{pmatrix} \frac{\Delta\Theta_1(t)}{\Delta\Theta_2(t-1)} & 0 \\ 0 & 1 \end{pmatrix} \tag{9}$$

1) IMPLEMENTING AND EVALUATING THE DATA ASSIMILATION ALGORITHM

(i) Background error covariance matrix

The parameters $\mathbf{B}$, $\mathbf{P}$ and $\mathbf{R}$ determine the relative weight given to the background, forecast

and to the observations covariance, respectively, while σ_{obs} corresponds to the observation (DisPATCh) error (see section *DisPATCh soil moisture data*). Observation errors are correlated in space. An accurate estimation of the background error is likely to be the most difficult task in the error prescription (Bouttier 1994; Reichle et al. 2002). Thus, a sensitivity analysis to background error on SSM and root zone soil moisture was carried out; a set of σ_{Θ_1} and σ_{Θ_2} were compared in order to estimate both background errors since there is no propagation equation of the background error covariance matrix using variational assimilation. In practice, an ensemble of 10 perturbations from 0.02 to 0.1 m^3 m^{-3} was built for both the background error terms and the global statistics (correlation coefficient r, Root Mean Square Error RMSE, and mean bias) were computed based on the analyzed and *in situ* SSM comparison. Results of the sensitivity study are displayed in Fig. 3. The optimal choices obtained from this sensitivity study were about 0.04 m^3 m^{-3} and 0.09 m^3 m^{-3} for σ_{Θ_1} and σ_{Θ_2}, respectively. Note that the same sensitivity study has been performed at 25 km, and the optimal choices obtained are 0.05 m^3 m^{-3} and 0.06 m^3 m^{-3} for σ_{Θ_1} and σ_{Θ_2}, respectively. Nevertheless, the range of bias and RMSE were low (about 0.009 m^3 m^{-3}) for the whole range of potential values. This means that the sensitivity analysis for both background errors presented limited choices. Interestingly, a Θ_1 background error lower than that of Θ_2 seems also consistent with the objective of the study, since Θ_2 was considered as a buffer variable to minimize biases on Θ_1. Finally, this quite low value of background error on Θ_1 was also certainly to be attributed to the good quality of ERA-interim data, which were the main forcing of the Θ_1 dynamics. Based on this analysis, the sub-optimal values of background error were chosen for the implementation of the data assimilation algorithm.

Fig. 3

(ii) Statistical metrics

It was important to assess the performance of the method, not only in terms of linear dependency and error, but also in terms of relative variability of the original and updated dataset. Therefore, r, RMSE, ubRMSE (unbiased-RMSE) and the mean bias were used to fully assess the accuracy of SSM (Entekhabi et al. 2010a). Moreover, a new metric called the Gain of DOWNscaling (GDOWN), introduced by Merlin et al. (2015), was also used. The gain is a measure of the statistical improvement dedicated to disaggregated SM products. The gain can range from -1 to 1, where positive values indicate better correspondence with *in situ* than low resolution products such as SMOS data. One key advantage of GDOWN, with regards to other performance metrics, is to provide an estimate of the overall improvement in soil moisture data with a single value.

4. Results and discussion

The DisPATCh/assimilation approach has been run over the entire year 2014 for both areas (Yanco in Australia and Tensift-Haouz in Morocco). First, ERA-interim precipitation products were assessed and validated using ground measurements. After, the analyzed SSM was evaluated at the time of DisPATCh availability. Finally, the analyzed SSM was assessed for the entire year datasets.

a. ERA-interim precipitation assessment

Although the assimilation scheme can compensate error on precipitation input data, a good agreement of ERA-Interim with ground rainfall in term of frequency (instead of quantity) is preferable to update the SSM state on a daily basis. A preliminary comparison between ERA-interim precipitation and the station data showed that ERA-interim presented too frequent low rainfall events (between 0.1 and 3 mm/day). This has already been observed by Ibrahim et al.

(2012) and Diaconescu et al. (2015) over another semi-arid region in the West African Sahel. The general overestimation of wet days is due to the fact that precipitation in reanalyses is mainly model generated, and therefore highly related to forecast-model physical parameterizations (surface pressure, temperature and wind). In this study, the precipitation values during low rainfall events ($<$ 3 mm/day) were set to zero (Ibrahim et al. 2012; Diaconescu et al. 2015). After this pre-procesing, ERA-interim precipitation were in better agreement with local station data (not shown). The daily ERA-interim precipitations were compared to the *in situ* data using 24-h accumulation from the raw 30 minutes observations. Fig. 4 and Table 2 reported the annual amounts and differences between the two precipitation data sets for each site. With an average bias of 27 mm/year and a r of 0.48, ERA-interim annual amounts matched quite well the *in situ* observations considering the large resolution of ERA-interim data and the high spatial variability of precipitation in semi-arid regions. Apart from sites Yanco 10 and Sidi Rahal, biases remained below 40 mm/year. Fig. 4 and Table 2 showed also that timing was well reproduced at $\pm$ 1 day, based on the correlation coefficient value when using a 3-days accumulated precipitation. For instance, daily ERA-interim precipitations at the Sidi Rahal site were really well correlated (r of 0.93) with the ground measurements. Regarding Yanco 10 site, the daily r was low; however it increased greatly using the 3-days accumulated precipitation (from 0.18 to 0.51). These results were similar to results found in Balsamo et al. (2010). In particular, none of the big storms events recorded by the local stations were missed by ERA-interim. Both timing and event amount were particularly well reproduced on Yanco 1 and 2. Two anomalies were noted at the Sidi Rahal site: the ERA-interim precipitation was underestimated compared with in situ observations, whereas the ERA-interim precipitation was overestimated at Yanco 10 station. For both sites, all events were well detected but the amounts of water were under and overestimated for Sidi Rahal and Yanco 10 sites, respectively. On average, ERA-interim precipitation data compared quite well

with *in situ* stations apart from moderated biases. The ERA-interim data set was thus used in the data assimilation algorithm in order to evaluate the performance of the approach when precipitation data are inaccurate, which is a very likely situation when no meteorological station is available.

Fig. 4 and Table 2

b. Assimilation results

Herein, the performance of the approach was assessed by comparing SMOS, DisPATCh, open loop and analyzed SSM with *in situ* measurements at the time of DisPATCh availability, in order to check if the analyzed SSM shows an improvement with regards to disaggregated SSM. All statistics were estimated on a yearly basis to evaluate the capability of a dynamical model to interpolate and, potentially, to improve DisPATCh SSM data. Table 3 showed the yearly statistics for each monitoring station and the number of comparison days. In this section, the number of days used was strongly dependent on the number of SMOS overpasses and cloud coverage. When comparing the statistics obtained over both areas, it was observed that the disaggregation and the assimilation scheme reduced bias by approximately 0.02 m^3 m^{-3}, while r was systematically higher after data assimilation. The disaggregation at 1 km (DisPATCh) has the advantage to produce SSM at a spatial resolution closer to the representativeness scale of ground measurements; it has been shown that this reduces the bias (Malbéteau et al. 2016). The mean r over the Yanco area rose from 0.62 to 0.77 after disaggregation and up to 0.80 after application of the assimilation scheme. Regarding Yanco 2, r improved from 0.69 to 0.79; bias reduced from 0.03 to 0.01 m^3 m^{-3} and ubRMSE decreased from 0.07 to 0.05 m^3 m^{-3}. Similar results were observed for Sidi Rahal as r increased from 0.82 to 0.87 after assimilation while

bias was closer to 0, and ubRMSE decreased slightly from 0.05 to 0.04 m^3 m^{-3}. Across all sites, the assimilation scheme does not improve significantly SSM in terms of statistics when using a limited (DiPATCh) time series for validation. Differences can be appreciated more easily through qualitative inspection of scatter plots. Sidi Rahal (Fig. 5b), Yanco 9 (Fig. 6b) and Yanco 10 (Fig. 7b) illustrate the Table 3 results. In these three plots, the analyzed distribution appears closer and more symmetric around the 1:1 line than for both DisPATCh and open loop.

As illustrated in Table 4, GDOWN was approximately equal for both the disaggregated and the analyzed data. Moreover the only site with negative values (meaning that SMOS shows better results) was Yanco 12, because DisPATCh and the analyzed SSM had a larger mean bias than SMOS (Table 3). However, r was slightly improved after assimilation, which means that the SSM dynamics were better represented. Yanco 2 was the site with the best enhanced GDOWN, with values going from 0.35 to 0.53 before and after assimilation, respectively. This was mainly due to a large improvement of r (from 0.47 to 0.79) and of the bias (from -0.03 m^3 m^{-3} to -0.01 m^3 m^{-3}). The assimilation scheme was also compared to the open loop estimates using the same statistics (Table 3). The assimilation clearly outperformed the open-loop prediction at the time of DisPATCh availability.

As a summary, this new approach improved the r values and also reduced the ubRMSE with regards to either the satellite observations or the model open loop, indicating that the assimilation has the capability to improve the SSM estimates over the model results or DisPATCh alone.

Table 3, Table 4, Fig. 5, Fig. 6 and Fig. 7

c. Soil moisture analysis

In order to assess the potential of using the force-restore model and the assimilation scheme for infilling disaggregated SSM, a conventional validation strategy was adopted, by comparing the analyzed and *in situ* SSM datasets for the full time series. This strategy was useful to characterize the overall quality of the analyzed SSM over both areas. The open loop estimate of SSM estimates determined from the force restore-model forced by ERA-interim were also computed for comparison purposes, along with the assimilation scheme applied to the original SMOS L3 product. This comparison evaluated the contribution of fine (instead of coarse) resolution soil moisture data. Table 5 displays temporal statistics for open loop, analyzed 25 km and analyzed 1 km SSM estimates for all *in situ* stations. Overall results showed that r was about 0.7, while mean bias was equal to 0.03 m^3 m^{-3} and ubRMSE was 0.06 m^3 m^{-3} for the analyzed SSM estimates. The r values were found to be systematically higher after assimilation, whereas bias, RMSE and ubRMSE were equivalent for both data sets. Regarding Sidi Rahal station (Fig. 5 and Table 5), r after data assimilation was about 0.83, while bias was close to 0.01 m^3 m^{-3} and the ubRMSE was around 0.06 m^3 m^{-3}. The time series exhibited the dominant seasonal cycle very well and showed a similar dynamical response to precipitation events. Comparison between analyzed 25 km and 1 km statistics showed that DisPATCh SSM improved results for all sites, even though the original SMOS L3 data had a larger temporal repetition. In others words, the spatial information provided by DisPATCh provide superior assimilation results despite the data gaps associated with cloud coverage over the study sites. Figs. 6 and 7 illustrate time series for two sites in the Yanco area. Regarding Yanco 10 (Fig. 7a), data assimilation enhanced r from 0.47 to 0.70, whereas the bias was larger by approximately 0.01 m^3 m^{-3}. The open loop SSM estimates showed a threshold for dry conditions at around 0.1 m^3 m^{-3} due to Θ_2 being forced

to 0.1 m^3 m^{-3} by lack of information. The analyzed SSM was not constrained any more by this artificial threshold. This demonstrated the importance of the analysis of Θ_2 for a correct estimate of Θ_1. Interestingly, the best improvement was observed for the irrigated site Yanco 9 (Fig. 6a) where precipitation was supplemented by irrigation inputs that were not taken into account in the model run. Consequently, the assimilation of DisPATCh data improved r (from 0.42 to 0.74), while bias, RMSE and ubRMSE were similarly compared to open loop results. The time series in Fig. 6a showed water input events at day 140 and day 325 (for example) that were certainly due to irrigation. Thus this approach could be used to detect and retrieve irrigation information that is very difficult to obtain over large areas on a daily basis. This information is requested by managers to monitor and control irrigation, especially for the monitoring of groundwater (Le Page et al. 2012).

The coupled scheme has the advantage of combining the spatial (but static) information provided by DisPATCh data with the temporal (but mono-dimensional) information provided by the force-restore scheme, in order to get SSM estimates every day at 1 km (Merlin et al. 2006). Fig. 8 and Fig. 9 showed the temporal average of SSM during one year over the Yanco area and the Tensift-Haouz basin, respectively. The irrigated areas are indicated for comparison purposes. Regarding the Australian case study, the Murrumbidgee river banks and irrigated areas appeared wetter than the dry grassland. The wet area located in the south of the study area is the floodplain of the Yanco Creek System, which is a tributary of the Murrumbidgee River downstream of Narrandera, flowing south-west. Over the Tensift-Haouz basin, the wetter pixels were mainly located in the irrigated areas. Nevertheless, it is important to keep in mind that the irrigated areas indicated may be inaccurate since many boreholes have been dug since the beginning of the 2000s, and they are neither registered nor monitored. A wet zone was also shown in the south

east of the study area. This region corresponds to the Atlas Mountain and its piedmont. A large amount of water in the piedmont is provided by the water from Atlas snowmelt (Boudhar et al. 2009). However, it is necessary to note that DisPATCh data may be unreliable in mountainous areas as the illumination effect on LST can be significant in steep-sided valleys (Malbéteau et al. 2017), and no correction for such effects has been included in DisPATCh yet (Molero et al. 2016). Note that the disaggregation images (fig. 8 and 9) present a slight boxy artifact at low (SMOS) resolution. Such an artifact is typical of downscaling methods like DisPATCh that apply a conservation law at low resolution (meaning that the average of disaggregated SM at SMOS resolution is set to SMOS observation).

Table 5, Fig. 8 and Fig. 9

As a summary, the proposed downscaling/assimilation scheme showed systematically higher r values with regards to the open loop and with regards to DisPATCh alone, indicating that the dynamic of the SSM at a daily time scale has been improved. The maps of yearly average SSM were consistent with the main hydrological characteristics of both catchment (rivers, wetlands and irrigated areas). This opens perspectives for the retrieval of irrigation water inputs.

5. Conclusion

The DisPATCh algorithm has been developed to improve the spatial resolution of readily available passive microwave-derived SSM data that is too coarse for many hydrological and agricultural applications. However, the temporal resolution of DisPATCh data based on SMOS and MODIS data is limited by the data gaps in MODIS images due to cloud cover, and by the temporal resolution of SMOS. This paper evaluated the potential of assimilating DisPATCh data

into the force-restore soil moisture model, forced by the ERA-interim precipitation data in order to obtain daily SSM at 1 km resolution. A variational scheme was used for root-zone soil moisture analysis taken as a buffer variable, together with a sequential approach for the update of SSM. The approach was tested during a one year period (2014) over two semi arid regions: 1) the Yanco zone in Australia and 2) the Tensift-Haouz basin in Morocco.

The performance of the data assimilation was first evaluated at the time of DisPATCh availability in order to check if the analyzed SSM showed an improvement with regards to the original products. Results showed that the analyzed SSM series were closer to the *in situ* measurement than DisPATCh (1 km resolution), model open loop (12.5 km resolution) and L3 SMOS SSM estimates (25 km resolution). The temporal statistics, when DisPATCh data were available, indicate an increase of r from 0.61 to 0.77 for downscaled data and up to 0.81 after assimilation. The bias was also reduced from 0.04 to 0.02 m^3 m^{-3} after downscaling, and ubRMSE decreased from 0.07 to 0.06 m^3 m^{-3} after assimilation of DisPATCh. The second step consisted in evaluating the analyzed SSM for the full time-series in order to assess the potential of interpolating SSM when the DisPATCh data was not available. The assimilation of DisPATCh data into the simple LSM improved quasi systematically the dynamic of the SSM with respect to the open-loop, as evidenced by enhanced r (from 0.53 to 0.70) and ubRMSE (from 0.07 to 0.06 m^3 m^{-3}). These results showed that the disaggregated SSM was able to improve the representation of the surface processes occurring at both fine and coarse scales, even when coarse scale and inaccurate meteorological data including rainfall were used. These results corroborate the study of Merlin et al. (2006), based on synthetic data showing that assimilation of a SSM downscaled product can compensate error on precipitation input data for the monitoring of SSM. Another interesting result was that the maps of yearly average SSM were consistent with the main hydrological char-

acteristics of both catchment (rivers, wetlands and irrigated areas). As future work, this approach will be applied and evaluated using the entire time series of SMOS/DisPATCh (6 years) to capture the inter-annual variability, and on other validation sites covering different eco-climatic conditions.

This study opens perspectives for developing new remote sensing-based methods in order to retrieve irrigation water inputs at 1 km resolution, and/or to improve precipitation estimates. In particular, several studies have been undertaken to estimate and/or improve precipitation estimates based on remotely sensed coarse-scale SSM (Brocca et al. 2013, 2014; Pellarin et al. 2008, 2013). A continuous SSM data in space and time could allow the disaggregation of coarse-scale precipitation data from re-analysis data sets at 1 km resolution for hydrological and agronomical applications. Likewise, 1 km daily irrigation input data set could help improve knowledge on how water is used for irrigation purposes.

Acknowledgments. This study was supported by the MIXMOD-E project (ANR-13-JS06-0003-01), funded by the French agency ANR (Agence Nationale de la Recherche), and as well the REC project (RISE-2014-645642- REC), funded by the European H2020 program. Initial setup and maintenance of the Murrumbidgee monitoring network used in this study was funded by the Australian Research Council (DP0343778, DP0557543, DP0879212, DP0984586, DP140100572) and by the CRC for Catchment Hydrology. Sidi Rahal station was funded by the MISTRAL METASIM/SICMED project and it is managed in the framework of the Joint International Laboratory TREMA http://trema.ucam.ac.ma.

References

Albergel, C., and Coauthors, 2008: From near-surface to root-zone soil moisture using an exponential filter: an assessment of the method based on in-situ observations and model sim-

ulations. *Hydrology and Earth System Sciences Discussions*, **5 (3)**, 1603–1640, doi:10.5194/hessd-5-1603-2008.

Allen, R., 2000: Using the FAO-56 dual crop coefficient method over an irrigated region as part of an evapotranspiration intercomparison study. *Journal of Hydrology*, **229 (1-2)**, 27–41, doi:10.1016/S0022-1694(99)00194-8.

Allen, R. G., L. S. Pereira, D. Raes, and M. Smith, 1998: Crop evapotranspiration- guidelines fo computing crop water requirements. *FAO Irrigation and Drainage Paper*, **56**, 1–15.

Allen, R. G., L. S. Pereira, M. Smith, D. Raes, and J. L. Wright, 2005: FAO-56 Dual Crop Coefficient Method for Estimating Evaporation from Soil and Application Extensions. *Journal of Irrigation and Drainage Engineering*, **131 (1)**, 2–13, doi:10.1061/(ASCE)0733-9437(2005)131:1(2).

Alvarez-Garreton, C., D. Ryu, A. W. Western, C. H. Su, W. T. Crow, D. E. Robertson, and C. Leahy, 2015: Improving operational flood ensemble prediction by the assimilation of satellite soil moisture: Comparison between lumped and semi-distributed schemes. *Hydrology and Earth System Sciences*, **19 (4)**, 1659–1676, doi:10.5194/hess-19-1659-2015.

Balsamo, G., S. Boussetta, P. Lopez, and L. Ferranti, 2010: Evaluation of ERA-Interim and ERA-Interim-GPCP-rescaled precipitation over the U.S.A. Shinfield Park, Reading, 25 pp.

Balsamo, G., F. Bouyssel, and J. Noilhan, 2004: A simplified bi-dimensional variational analysis of soil moisture from screen-level observations in a mesoscale numerical weather-prediction model. *Quarterly Journal of the Royal Meteorological Society*, **130**, 895–915, doi:10.1256/qj.02.215.

572 Balsamo, G., and Coauthors, 2015: ERA-Interim/Land: a global land surface reanalysis data set.
573 *Hydrology and Earth System Sciences*, **19 (1)**, 389–407, doi:10.5194/hess-19-389-2015.

574 Bandara, R., J. P. Walker, C. Rüdiger, and O. Merlin, 2015: Towards soil property retrieval from
575 space: An application with disaggregated satellite observations. *Journal of Hydrology*, **522**,
576 582–593, doi:10.1016/j.jhydrol.2015.01.018.

577 Bao, X., and F. Zhang, 2013: Evaluation of NCEP-CFSR, NCEP-NCAR, ERA-Interim, and ERA-
578 40 reanalysis datasets against independent sounding observations over the Tibetan Plateau. *Jour-*
579 *nal of Climate*, **26 (1)**, 206–214, doi:10.1175/JCLI-D-12-00056.1.

580 Belo-Pereira, M., E. Dutra, and P. Viterbo, 2011: Evaluation of global precipitation data sets
581 over the Iberian Peninsula. *Journal of Geophysical Research*, **116 (D20)**, D20 101, doi:10.1029/
582 2010JD015481.

583 Beven, K., 1989: Changing ideas in hydrology - The case of physically-based models. *Journal of*
584 *Hydrology*, **105 (1-2)**, 157–172, doi:10.1016/0022-1694(89)90101-7, arXiv:1011.1669v3.

585 Boisvert, L. N., D. L. Wu, T. Vihma, and J. Susskind, 2015: Verification of air/surface humidity
586 differences from AIRS and ERA-Interim in support of turbulent flux estimation in the Arctic.
587 *Journal of Geophysical Research: Atmospheres*, **120 (3)**, 945–963, doi:10.1002/2014JD021666.

588 Boudhar, A., L. Hanich, G. Boulet, B. Duchemin, B. Berjamy, and A. Chehbouni, 2009: Eval-
589 uation of the Snowmelt Runoff Model in the Moroccan High Atlas Mountains using two
590 snow-cover estimates. *Hydrological Sciences Journal*, **54 (March 2015)**, 1094–1113, doi:
591 10.1623/hysj.54.6.1094.

592 Bouttier, F., 1994: A Dynamical Estimation of Forecast Error Covariances in an Assimilation Sys-
593 tem. *Monthly Weather Review*, **122 (10)**, 2376–2390, doi:10.1175/1520-0493(1994)122⟨2376:
594 ADEOFE⟩2.0.CO;2.

595 Brocca, L., T. Moramarco, F. Melone, and W. Wagner, 2013: A new method for rainfall estimation
596 through soil moisture observations. *Geophysical Research Letters*, **40 (5)**, 853–858, doi:10.
597 1002/grl.50173, 1403.6496.

598 Brocca, L., T. Moramarco, F. Melone, W. Wagner, S. Hasenauer, and S. Hahn, 2012: Assimilation
599 of surface- and root-zone ASCAT soil moisture products into rainfall-runoff modeling. *IEEE*
600 *Transactions on Geoscience and Remote Sensing*, **50 (7 PART1)**, 2542–2555, doi:10.1109/
601 TGRS.2011.2177468.

602 Brocca, L., and Coauthors, 2014: Soil as a natural rain gauge: Estimating global rainfall from
603 satellite soil moisture data. *Journal of Geophysical Research: Atmospheres*, **119 (9)**, 5128–
604 5141, doi:10.1002/2014JD021489.

605 Calvet, J.-C., J. Noilhan, and P. Bessemoulin, 1998: Retrieving the Root-Zone Soil Moisture from
606 Surface Soil Moisture or Temperature Estimates: A Feasibility Study Based on Field Mea-
607 surements. *Journal of Applied Meteorology*, **37 (4)**, 371–386, doi:10.1175/1520-0450(1998)
608 037⟨0371:RTRZSM⟩2.0.CO;2.

609 Ceballos, A., K. Scipal, W. Wagner, and J. Martínez-Fernández, 2005: Validation of ERS
610 scatterometer-derived soil moisture data in the central part of the Duero Basin, Spain. *Hydro-*
611 *logical Processes*, **19 (8)**, 1549–1566, doi:10.1002/hyp.5585.

612 Chehbouni, A., and Coauthors, 2008: An integrated modelling and remote sensing approach for
613 hydrological study in arid and semiarid regions: the SUDMED Programme. *International Jour-*

nal of Remote Sensing, **29 (17-18)**, 5161–5181, doi:10.1080/01431160802036417.

Chen, F., W. T. Crow, and D. Ryu, 2014: Dual Forcing and State Correction via Soil Moisture Assimilation for Improved RainfallRunoff Modeling. *Journal of Hydrometeorology*, **15 (5)**, 1832–1848, doi:10.1175/JHM-D-14-0002.1.

Crow, W. T., and E. F. Wood, 2003: The assimilation of remotely sensed soil brightness temperature imagery into a land surface model using Ensemble Kalman filtering: A case study based on ESTAR measurements during SGP97. *Advances in Water Resources*, **26 (2)**, 137–149, doi:10.1016/S0309-1708(02)00088-X.

Das, N. N., D. Entekhabi, E. G. Njoku, J. J. C. Shi, J. T. Johnson, and A. Colliander, 2014: Tests of the SMAP Combined Radar and Radiometer Algorithm Using Airborne Field Campaign Observations and Simulated Data. *IEEE Transactions on Geoscience and Remote Sensing*, **52 (4)**, 2018–2028, doi:10.1109/TGRS.2013.2257605.

De Lannoy, G. J. M., and R. H. Reichle, 2016: Assimilation of SMOS brightness temperatures or soil moisture retrievals into a land surface model. *Hydrology and Earth System Sciences*, **20 (12)**, 4895–4911, doi:10.5194/hess-20-4895-2016.

De Lannoy, G. J. M., R. H. Reichle, K. R. Arsenault, P. R. Houser, S. Kumar, N. E. C. Verhoest, and V. R. N. Pauwels, 2012: Multiscale assimilation of Advanced Microwave Scanning Radiometer-EOS snow water equivalent and Moderate Resolution Imaging Spectroradiometer snow cover fraction observations in northern Colorado. *Water Resources Research*, **48 (1)**, doi:10.1029/2011WR010588, URL http://doi.wiley.com/10.1029/2011WR010588.

De Lannoy, G. J. M., R. H. Reichle, P. R. Houser, K. R. Arsenault, N. E. C. Verhoest, and V. R. N. Pauwels, 2010: Satellite-Scale Snow Water Equivalent Assimilation into a

636 High-Resolution Land Surface Model. *Journal of Hydrometeorology*, **11 (2)**, 352–369, doi:
637 10.1175/2009JHM1192.1, URL http://journals.ametsoc.org/doi/abs/10.1175/2009JHM1192.1.

638 Deardorff, J. W., 1977: A Parameterization of Ground-Surface Moisture Content for Use in
639 Atmospheric Prediction Models. *Journal of Applied Meteorology*, **16 (11)**, 1182–1185, doi:
640 10.1175/1520-0450(1977)016⟨1182:APOGSM⟩2.0.CO;2.

641 Dee, D. P., and Coauthors, 2011: The ERA-Interim reanalysis: Configuration and performance of
642 the data assimilation system. *Quarterly Journal of the Royal Meteorological Society*, **137 (656)**,
643 553–597, doi:10.1002/qj.828.

644 Demaria, E. M., B. Nijssen, and T. Wagener, 2007: Monte Carlo sensitivity analysis of land surface
645 parameters using the Variable Infiltration Capacity model. *Journal of Geophysical Research*,
646 **112 (D11)**, D11 113, doi:10.1029/2006JD007534.

647 Diaconescu, E. P., P. Gachon, J. Scinocca, and R. Laprise, 2015: Evaluation of daily precipitation
648 statistics and monsoon onset/retreat over western Sahel in multiple data sets. *Climate Dynamics*,
649 **45 (5-6)**, 1325–1354, doi:10.1007/s00382-014-2383-2.

650 Djamai, N., R. Magagi, K. Goïta, O. Merlin, Y. Kerr, and A. Roy, 2016: A combination of
651 DISPATCH downscaling algorithm with CLASS land surface scheme for soil moisture es-
652 timation at fine scale during cloudy days. *Remote Sensing of Environment*, **184**, 1–14, doi:
653 10.1016/j.rse.2016.06.010.

654 Draper, C., J. F. Mahfouf, J. C. Calvet, E. Martin, and W. Wagner, 2011: Assimilation of ASCAT
655 near-surface soil moisture into the SIM hydrological model over France. *Hydrology and Earth*
656 *System Sciences*, **15 (12)**, 3829–3841, doi:10.5194/hess-15-3829-2011.

Dumedah, G., A. A. Berg, and M. Wineberg, 2011: An Integrated Framework for a Joint Assimilation of Brightness Temperature and Soil Moisture Using the Nondominated Sorting Genetic Algorithm II. *Journal of Hydrometeorology*, **12 (6)**, 1596–1609, doi:10.1175/JHM-D-10-05029.1.

Dumedah, G., and J. P. Walker, 2014: Evaluation of Model Parameter Convergence when Using Data Assimilation for Soil Moisture Estimation. *Journal of Hydrometeorology*, **15 (1)**, 359–375, doi:10.1175/JHM-D-12-0175.1.

Dumedah, G., J. P. Walker, and O. Merlin, 2015: Root-zone soil moisture estimation from assimilation of downscaled Soil Moisture and Ocean Salinity data. *Advances in Water Resources*, **84**, 14–22, doi:10.1016/j.advwatres.2015.07.021.

Entekhabi, D., 1995: Recent advances in land-atmosphere interaction research. *Reviews of Geophysics*, **33 (95)**, 995, doi:10.1029/95RG01163.

Entekhabi, D., H. Nakamura, and E. Njoku, 1994: Solving the inverse problem for soil moisture and temperature profiles by sequential assimilation of multifrequency remotely sensed observations. *IEEE Transactions on Geoscience and Remote Sensing*, **32 (2)**, 438–448, doi:10.1109/36.295058.

Entekhabi, D., R. H. Reichle, R. D. Koster, and W. T. Crow, 2010a: Performance Metrics for Soil Moisture Retrievals and Application Requirements. *Journal of Hydrometeorology*, **11 (3)**, 832–840, doi:10.1175/2010JHM1223.1.

Entekhabi, D., and Coauthors, 2010b: The Soil Moisture Active Passive (SMAP) Mission. *Proceedings of the IEEE*, **98 (5)**, 704–716, doi:10.1109/JPROC.2010.2043918.

Escorihuela, M. J., and P. Quintana-Seguí, 2016: Comparison of remote sensing and simulated soil moisture datasets in Mediterranean landscapes. *Remote Sensing of Environment*, **180**, 99–114, doi:10.1016/j.rse.2016.02.046.

Fang, B., V. Lakshmi, R. Bindlish, T. J. Jackson, M. Cosh, and J. Basara, 2013: Passive Microwave Soil Moisture Downscaling Using Vegetation Index and Skin Surface Temperature. *Vadose Zone Journal*, **12 (3)**, doi:10.2136/vzj2013.05.0089.

Franks, S. W., K. J. Beven, P. F. Quinn, and I. R. Wright, 1997: On the sensitivity of soil-vegetation-atmosphere transfer (SVAT) schemes: Equifinality and the problem of robust calibration. *Agricultural and Forest Meteorology*, **86 (1-2)**, 63–75, doi:10.1016/S0168-1923(96)02421-5.

Gao, X., P. Wu, X. Zhao, J. Wang, and Y. Shi, 2014: Effects of land use on soil moisture variations in a semi-arid catchment: implications for land and agricultural water management. *Land Degradation & Development*, **25 (2)**, 163–172, doi:10.1002/ldr.1156.

Gutman, G., and A. Ignatov, 1998: The derivation of the green vegetation fraction from NOAA/AVHRR data for use in numerical weather prediction models. *International Journal of Remote Sensing*, **19 (8)**, 1533–1543, doi:10.1080/014311698215333.

Ibrahim, B., J. Polcher, H. Karambiri, and B. Rockel, 2012: Characterization of the rainy season in Burkina Faso and it's representation by regional climate models. *Climate Dynamics*, **39 (6)**, 1287–1302, doi:10.1007/s00382-011-1276-x.

Jackson, T. J., T. J. Schugge, A. D. Nicks, G. A. Coleman, and E. T. Engman, 1981: Soil moisture updating and microwave remote sensing for hydrological simulation / La remise à jour de

l'état d'humidité des sols en vue de la simulation hydrologique. *Hydrological Sciences Bulletin*, **26 (3)**, 305–319, doi:10.1080/02626668109490889.

Jacquette, E., Y. Kerr, A. Al Bitar, F. Cabot, A. Mialon, P. Richaume, A. Quesney, and L. Berthon, 2013: CATDS SMOS L3 soil moisture retrieval processor, Algorithm Theoretical Baseline Document (ATBD). *Toulouse CESBIO*.

Jarlan, L., G. Balsamo, S. Lafont, A. Beljaars, J. C. Calvet, and E. Mougin, 2008: Analysis of leaf area index in the ECMWF land surface model and impact on latent heat and carbon fluxes : Application to West Africa. **113 (December)**, 1–22, doi:10.1029/2007JD009370.

Jarlan, L., and Coauthors, 2015: Remote Sensing of Water Resources in Semi-Arid Mediterranean Areas: the joint international laboratory TREMA. *International Journal of Remote Sensing*, **36 (19-20)**, 4879–4917, doi:10.1080/01431161.2015.1093198.

Kerr, Y., and Coauthors, 2014: CATDS LEVEL 3 - Soil Moisture and Brightness Temperature -.

Kerr, Y. H., 2007: Soil moisture from space: Where are we? *Hydrogeology Journal*, **15 (1)**, 117–120, doi:10.1007/s10040-006-0095-3.

Kerr, Y. H., and Coauthors, 2012: The SMOS Soil Moisture Retrieval Algorithm. *IEEE Transactions on Geoscience and Remote Sensing*, **50 (5)**, 1384–1403, doi:10.1109/TGRS.2012.2184548.

Kim, J., and T. S. Hogue, 2012: Improving Spatial Soil Moisture Representation Through Integration of AMSR-E and MODIS Products. *IEEE Transactions on Geoscience and Remote Sensing*, **50 (2)**, 446–460, doi:10.1109/TGRS.2011.2161318.

Kim, S., 2013: Ancillary Data Report Landcover Classification. **(042)**.

719 Kumar, S. V., and Coauthors, 2014: Assimilation of remotely sensed soil moisture and snow
720 depth retrievals for drought estimation. *Journal of Hydrometeorology*, 140603130821005, doi:
721 10.1175/JHM-D-13-0132.1.

722 Le Page, M., and Coauthors, 2012: An Integrated DSS for Groundwater Management Based on
723 Remote Sensing. The Case of a Semi-arid Aquifer in Morocco. *Water Resources Management*,
724 **26 (11)**, 3209–3230, doi:10.1007/s11269-012-0068-3.

725 Leroux, D. J., and Coauthors, 2016: Assimilation of SMOS soil moisture into a distributed hy-
726 drological model and impacts on the water cycle variables over the Ouémé catchment in Benin.
727 *Hydrology and Earth System Sciences*, **20 (7)**, 2827–2840, doi:10.5194/hess-20-2827-2016.

728 Lievens, H., B. Martens, N. Verhoest, S. Hahn, R. Reichle, and D. Miralles, 2017: Assimilation
729 of global radar backscatter and radiometer brightness temperature observations to improve soil
730 moisture and land evaporation estimates. *Remote Sensing of Environment*, **189**, 194–210, doi:
731 10.1016/j.rse.2016.11.022.

732 Lievens, H., and Coauthors, 2015a: Assimilation of SMOS soil moisture and brightness tem-
733 perature products into a land surface model. *Remote Sensing of Environment*, **180**, 292–304,
734 doi:10.1016/j.rse.2015.10.033.

735 Lievens, H., and Coauthors, 2015b: SMOS soil moisture assimilation for improved hydrologic
736 simulation in the Murray Darling Basin, Australia. *Remote Sensing of Environment*, **168**, 146–
737 162, doi:10.1016/j.rse.2015.06.025.

738 Lievens, H., and Coauthors, 2016: Assimilation of SMOS soil moisture and brightness tempera-
739 ture products into a land surface model. *Remote Sensing of Environment*, **180**, 292–304, doi:10.
740 1016/j.rse.2015.10.033, URL http://linkinghub.elsevier.com/retrieve/pii/S003442571530184X.

741 Malbéteau, Y., O. Merlin, S. Gascoin, J. Gastellu, C. Mattar, L. Olivera-Guerra, S. Khabba, and
742 L. Jarlan, 2017: Normalizing land surface temperature data for elevation and illumination effects
743 in mountainous areas: A case study using ASTER data over a steep-sided valley in Morocco.
744 *Remote Sensing of Environment*, **189**, 25–39, doi:10.1016/j.rse.2016.11.010.

745 Malbéteau, Y., O. Merlin, B. Molero, C. Rüdiger, and S. Bacon, 2016: DisPATCh as a tool to eval-
746 uate coarse-scale remotely sensed soil moisture using localized in situ measurements: Appli-
747 cation to SMOS and AMSR-E data in Southeastern Australia. *International Journal of Applied*
748 *Earth Observation and Geoinformation*, **45**, 221–234, doi:10.1016/j.jag.2015.10.002.

749 Margulis, S. a., D. B. Mclaughlin, D. Entekhabi, and S. Dunne, 2002: Land data assimilation
750 and estimation of soil moisture using measurements from the Southern Great Plains 1997 Field
751 Experiment. *Water Resources Research*, **38 (12)**, 1–18, doi:10.1029/2001WR001114.

752 Massari, C., L. Brocca, A. Tarpanelli, and T. Moramarco, 2015: *Data assimilation of satellite*
753 *soil moisture into rainfall-runoffmodelling: A complex recipe?*, Vol. 7. 11403–11433 pp., doi:
754 10.3390/rs70911403.

755 Merlin, O., A. Chehbouni, G. Boulet, and Y. Kerr, 2006: Assimilation of Disaggregated Mi-
756 crowave Soil Moisture into a Hydrologic Model Using Coarse-Scale Meteorological Data. *Jour-*
757 *nal of Hydrometeorology*, **7 (6)**, 1308–1322, doi:10.1175/JHM552.1.

758 Merlin, O., A. Chehbouni, J. Walker, R. Panciera, and Y. Kerr, 2008a: A Simple Method to
759 Disaggregate Passive Microwave-Based Soil Moisture. *IEEE Transactions on Geoscience and*
760 *Remote Sensing*, **46 (3)**, 786–796, doi:10.1109/TGRS.2007.914807.

761 Merlin, O., M. J. Escorihuela, M. A. Mayoral, O. Hagolle, A. Al Bitar, and Y. Kerr, 2013: Self-
762 calibrated evaporation-based disaggregation of SMOS soil moisture: An evaluation study at

763 3km and 100m resolution in Catalunya, Spain. *Remote Sensing of Environment*, **130**, 25–38,
764 doi:10.1016/j.rse.2012.11.008.

765 Merlin, O., Y. Malbéteau, Y. Notfi, S. Bacon, S. Khabba, and L. Jarlan, 2015: Performance Metrics
766 for Soil Moisture Downscaling Methods: Application to DISPATCH Data in Central Morocco.
767 *Remote Sensing*, **7 (4)**, 3783–3807, doi:10.3390/rs70403783.

768 Merlin, O., C. Rudiger, A. Al Bitar, P. Richaume, J. P. Walker, and Y. H. Kerr, 2012: Disaggrega-
769 tion of SMOS Soil Moisture in Southeastern Australia. *IEEE Transactions on Geoscience and*
770 *Remote Sensing*, **50 (5)**, 1556–1571, doi:10.1109/TGRS.2011.2175000.

771 Merlin, O., and Coauthors, 2008b: The NAFE'06 data set: Towards soil moisture retrieval at inter-
772 mediate resolution. *Advances in Water Resources*, **31 (11)**, 1444–1455, doi:10.1016/j.advwatres.
773 2008.01.018.

774 Mladenova, I., V. Lakshmi, T. J. Jackson, J. P. Walker, O. Merlin, and R. A. de Jeu, 2011:
775 Validation of AMSR-E soil moisture using L-band airborne radiometer data from National
776 Airborne Field Experiment 2006. *Remote Sensing of Environment*, **115 (8)**, 2096–2103, doi:
777 10.1016/j.rse.2011.04.011.

778 Molero, B., and Coauthors, 2016: SMOS disaggregated soil moisture product at 1 km resolution:
779 Processor overview and first validation results. *Remote Sensing of Environment*, **180**, 361–376,
780 doi:10.1016/j.rse.2016.02.045.

781 Mooney, P. A., F. J. Mulligan, and R. Fealy, 2011: Comparison of ERA-40, ERA-Interim and
782 NCEP/NCAR reanalysis data with observed surface air temperatures over Ireland. *International*
783 *Journal of Climatology*, **31 (4)**, 545–557, doi:10.1002/joc.2098.

Njoku, E. G., and D. Entekhabi, 1996: Passive microwave remote sensing of soil moisture. *Journal of Hydrology*, **184 (1-2)**, 101–129, doi:10.1016/0022-1694(95)02970-2.

Noilhan, J., and J.-F. Mahfouf, 1996: The ISBA land surface parameterisation scheme. *Global and Planetary Change*, **13 (1-4)**, 145–159, doi:10.1016/0921-8181(95)00043-7.

Noilhan, J., and S. Planton, 1989: A Simple Parameterization of Land Surface Processes for Meteorological Models. *Monthly Weather Review*, **117 (3)**, 536–549, doi:10.1175/1520-0493(1989)117⟨0536:ASPOLS⟩2.0.CO;2.

Pan, M., E. F. Wood, D. B. McLaughlin, D. Entekhabi, and L. Luo, 2009a: A Multiscale Ensemble Filtering System for Hydrologic Data Assimilation. Part I: Implementation and Synthetic Experiment. *Journal of Hydrometeorology*, **10 (3)**, 794–806, doi:10.1175/2009JHM1088.1.

Pan, M., E. F. Wood, D. B. McLaughlin, D. Entekhabi, and L. Luo, 2009b: A Multiscale Ensemble Filtering System for Hydrologic Data Assimilation. Part I: Implementation and Synthetic Experiment. *Journal of Hydrometeorology*, **10 (3)**, 794–806, doi:10.1175/2009JHM1088.1.

Panciera, R., and Coauthors, 2014: The Soil Moisture Active Passive Experiments (SMAPEx): Toward Soil Moisture Retrieval From the SMAP Mission. *IEEE Transactions on Geoscience and Remote Sensing*, **52 (1)**, 490–507, doi:10.1109/TGRS.2013.2241774.

Parada, L. M., and X. Liang, 2004: Optimal multiscale Kalman filter for assimilation of near-surface soil moisture into land surface models. *Journal of Geophysical Research D: Atmospheres*, **109 (24)**, 1–21, doi:10.1029/2004JD004745.

Pauwels, V. R. N., R. Hoeben, N. E. C. Verhoest, and F. P. De Troch, 2001: The importance of the spatial patterns of remotely sensed soil moisture in the improvement of discharge predictions

for small-scale basins through data assimilation. *Journal of Hydrology*, **251 (1-2)**, 88–102, doi: 10.1016/S0022-1694(01)00440-1.

Peischl, S., J. P. Walker, C. Rüdiger, N. Ye, Y. H. Kerr, E. Kim, R. Bandara, and M. Allahmoradi, 2012: The AACES field experiments: SMOS calibration and validation across the Murrumbidgee River catchment. *Hydrology and Earth System Sciences*, **16 (6)**, 1697–1708, doi:10.5194/hess-16-1697-2012.

Pellarin, T., A. Ali, F. Chopin, I. Jobard, and J.-C. Bergès, 2008: Using spaceborne surface soil moisture to constrain satellite precipitation estimates over West Africa. *Geophysical Research Letters*, **35 (2)**, L02 813, doi:10.1029/2007GL032243.

Pellarin, T., J.-C. Calvet, and W. Wagner, 2006: Evaluation of ERS scatterometer soil moisture products over a half-degree region in southwestern France. *Geophysical Research Letters*, **33 (17)**, L17 401, doi:10.1029/2006GL027231.

Pellarin, T., S. Louvet, C. Gruhier, G. Quantin, and C. Legout, 2013: A simple and effective method for correcting soil moisture and precipitation estimates using AMSR-E measurements. *Remote Sensing of Environment*, **136**, 28–36, doi:10.1016/j.rse.2013.04.011.

Pfeifroth, U., R. Mueller, and B. Ahrens, 2013: Evaluation of Satellite-Based and Reanalysis Precipitation Data in the Tropical Pacific. *Journal of Applied Meteorology and Climatology*, **52 (3)**, 634–644, doi:10.1175/JAMC-D-12-049.1.

Piles, M., A. Camps, M. Vall-llossera, I. Corbella, R. Panciera, C. Rudiger, Y. H. Kerr, and J. Walker, 2011: Downscaling SMOS-Derived Soil Moisture Using MODIS Visible/Infrared Data. *IEEE Transactions on Geoscience and Remote Sensing*, **49 (9)**, 3156–3166, doi:10.1109/TGRS.2011.2120615.

827 Reichle, R., D. McLaughlin, and D. Entekhabi, 2001a: Variational data assimilation of microwave
828 radiobrightness observations for land surface hydrology applications. *IEEE Transactions on*
829 *Geoscience and Remote Sensing*, **39 (8)**, 1708–1718, doi:10.1109/36.942549.

830 Reichle, R. H., W. T. Crow, and C. L. Keppenne, 2008: An adaptive ensemble Kalman filter for soil
831 moisture data assimilation. *Water Resources Research*, **44 (3)**, doi:10.1029/2007WR006357.

832 Reichle, R. H., D. Entekhabi, and D. B. McLaughlin, 2001b: Downscaling of radio brightness
833 measurements for soil moisture estimation: A four-dimensional variational data assimilation
834 approach. *Water Resources Research*, **37 (9)**, 2353–2364, doi:10.1029/2001WR000475, URL
835 http://doi.wiley.com/10.1029/2001WR000475.

836 Reichle, R. H., R. D. Koster, P. Liu, S. P. P. Mahanama, E. G. Njoku, and M. Owe, 2007:
837 Comparison and assimilation of global soil moisture retrievals from the Advanced Microwave
838 Scanning Radiometer for the Earth Observing System (AMSR-E) and the Scanning Multi-
839 channel Microwave Radiometer (SMMR). *Journal of Geophysical Research*, **112 (D9)**, doi:
840 10.1029/2006JD008033.

841 Reichle, R. H., S. V. Kumar, S. P. P. Mahanama, R. D. Koster, and Q. Liu, 2010: Assimila-
842 tion of Satellite-Derived Skin Temperature Observations into Land Surface Models. *Journal*
843 *of Hydrometeorology*, **11 (5)**, 1103–1122, doi:10.1175/2010JHM1262.1, URL http://journals.
844 ametsoc.org/doi/abs/10.1175/2010JHM1262.1.

845 Reichle, R. H., D. B. McLaughlin, and D. Entekhabi, 2002: Hydrologic Data Assimilation
846 with the Ensemble Kalman Filter. *Monthly Weather Review*, **130 (1)**, 103–114, doi:10.1175/
847 1520-0493(2002)130⟨0103:HDAWTE⟩2.0.CO;2.

Ridler, M.-E., H. Madsen, S. Stisen, S. Bircher, and R. Fensholt, 2014: Assimilation of SMOS-derived soil moisture in a fully integrated hydrological and soil-vegetation-atmosphere transfer model in Western Denmark. *Water Resources Research*, **50 (11)**, 8962–8981, doi: 10.1002/2014WR015392.

Rodriguez-Iturbe, I., 2000: Ecohydrology: A hydrologic perspective of climate-soil-vegetation dynamies. *Water Resources Research*, **36 (1)**, 3–9, doi:10.1029/1999WR900210.

Sabater, J. M., L. Jarlan, J.-C. Calvet, F. Bouyssel, and P. De Rosnay, 2007: From Near-Surface to Root-Zone Soil Moisture Using Different Assimilation Techniques. *Journal of Hydrometeorology*, **8 (2)**, 194–206, doi:10.1175/JHM571.1.

Sabater, J. M., C. Rüdiger, J.-c. Calvet, N. Fritz, L. Jarlan, and Y. Kerr, 2008: Joint assimilation of surface soil moisture and LAI observations into a land surface model. *Agricultural and Forest Meteorology*, **148 (8-9)**, 1362–1373, doi:10.1016/j.agrformet.2008.04.003.

Sahoo, A. K., G. J. De Lannoy, R. H. Reichle, and P. R. Houser, 2013: Assimilation and downscaling of satellite observed soil moisture over the Little River Experimental Watershed in Georgia, USA. *Advances in Water Resources*, **52**, 19–33, doi:10.1016/j.advwatres.2012.08.007, URL http://linkinghub.elsevier.com/retrieve/pii/S0309170812002357.

Sánchez-Ruiz, S., M. Piles, N. Sánchez, J. Martínez-Fernández, M. Vall-llossera, and A. Camps, 2014: Combining SMOS with visible and near/shortwave/thermal infrared satellite data for high resolution soil moisture estimates. *Journal of Hydrology*, **516**, 273–283, doi:10.1016/j.jhydrol.2013.12.047.

Sellers, P. J., Y. Mintz, Y. C. Sud, and A. Dalcher, 1986: A Simple Biosphere Model (SIB) for Use within General Circulation Models. *Journal of the Atmospheric Sciences*, **43 (6)**, 505–531,

doi:10.1175/1520-0469(1986)043⟨0505:ASBMFU⟩2.0.CO;2.

Smith, a. B., and Coauthors, 2012: The Murrumbidgee soil moisture monitoring network data set. *Water Resources Research*, **48 (7)**, doi:10.1029/2012WR011976.

Srivastava, P. K., D. Han, M. R. Ramirez, and T. Islam, 2013: Machine Learning Techniques for Downscaling SMOS Satellite Soil Moisture Using MODIS Land Surface Temperature for Hydrological Application. *Water Resources Management*, **27 (8)**, 3127–3144, doi:10.1007/s11269-013-0337-9.

Su, Z., P. de Rosnay, J. Wen, L. Wang, and Y. Zeng, 2013: Evaluation of ECMWF's soil moisture analyses using observations on the Tibetan Plateau. *Journal of Geophysical Research: Atmospheres*, **118 (11)**, 5304–5318, doi:10.1002/jgrd.50468.

Szczypta, C., J. C. Calvet, C. Albergel, G. Balsamo, S. Boussetta, D. Carrer, S. Lafont, and C. Meurey, 2011: Verification of the new ECMWF ERA-Interim reanalysis over France. *Hydrology and Earth System Sciences*, **15 (2)**, 647–666, doi:10.5194/hess-15-647-2011.

Vachaud, G., A. Passerat De Silans, P. Balabanis, and M. Vauclin, 1985: Temporal Stability of Spatially Measured Soil Water Probability Density Function. *Soil Science Society of America Journal*, **49 (4)**, 822, doi:10.2136/sssaj1985.03615995004900040006x.

Wagner, W., G. Lemoine, and H. Rott, 1999: A Method for Estimating Soil Moisture from ERS Scatterometer and Soil Data. *Remote Sensing of Environment*, **70 (2)**, 191–207, doi:10.1016/S0034-4257(99)00036-X.

Wanders, N., D. Karssenberg, A. De Roo, S. M. De Jong, and M. F. P. Bierkens, 2014: The suitability of remotely sensed soil moisture for improving operational flood forecasting. *Hydrology and Earth System Sciences*, **18 (6)**, 2343–2357, doi:10.5194/hess-18-2343-2014.

892 Wang, A., and X. Zeng, 2012: Evaluation of multireanalysis products with in situ observations
893 over the Tibetan Plateau. *Journal of Geophysical Research Atmospheres*, **117 (5)**, 1–12, doi:
894 10.1029/2011JD016553.

895 Zhang, Q., H. Körnich, and K. Holmgren, 2013: How well do reanalyses represent the southern
896 African precipitation? *Climate Dynamics*, **40 (3-4)**, 951–962, doi:10.1007/s00382-012-1423-z.

LIST OF TABLES

TABLE 1. Main characteristics of validation sites.

Country	Station	Longitude WGS84 (°)	Latitude WGS84 (°)	Elevation (m)	Land use	SM 0-5 cm (% of obs)	Precipitation (mm)	Irrigation
Morocco	Sidi Rahal	-7.3535	31.7035	767	Dryland crop/grazing	91.5	398	
Australia	Yanco 1	145.8490	-34.6288	120	Dryland crop/grazing	67.7	294	X
	Yanco 2	146.1103	-34.6547	130	Grazing	100.0	323	
	Yanco 8	146.4140	-34.8470	149	Grazing	98.6	374	
	Yanco 9	146.0163	-34.9678	122	Crop	100.0	329	
	Yanco 10	146.3099	-35.0054	119	Grazing	95.3	368	
	Yanco 12	146.1689	-35.0696	120	Crop/grazing	79.2	345	
	Yanco 13	146.3065	-35.0903	121	Gazing	66.0	368	

913 TABLE 2. Comparison between *in situ* and ERA-interim precipitation: annual bias and correlation coefficient
914 r for accumulating precipitation of 1, 3, 5 and 10 days; n is the number of comparison days.

Country	Station	n	Precipitation *in situ*	Precipitation ECMWF	bias (mm)	r	r 3days	r 5days	r 10days
Morocco	Sidi Rahal	334	393	265.3	127.7	0.93	0.94	0.95	0.96
Australia	Yanco 1	245	294.6	258.7	35.9	0.44	0.6	0.62	0.63
	Yanco 2	365	358.6	323.3	35.3	0.48	0.59	0.6	0.59
	Yanco 8	No data	No data	350.8	No data	No data	No data	No data	No data
	Yanco 9	365	299.2	329.2	-30	0.5	0.64	0.67	0.66
	Yanco 10	342	187.6	327.3	-139.7	0.18	0.51	0.62	0.69
	Yanco 12	256	260.2	242.9	17.3	0.66	0.76	0.79	0.8
	Yanco 13	249	249.4	282.9	-33.5	0.59	0.69	0.72	0.74
	Average		274.9	302.2	-27.2	0.48	0.63	0.67	0.69

TABLE 3. Temporal statistics and their 95% confidence intervals are provided of all stations between SMOS L3, DisPATCh, open loop and analyzed SSM with respect to *in situ* measurement; r is the correlation coefficient, RMSE is the root mean square error, ubRMSE is the unbiased-RMSE and n is the number of comparison days. With a p-value <0.01 for all sites, statistics are significant.

			r				bias ($m^3\ m^{-3}$)				RMSE ($m^3\ m^{-3}$)				ubRMSE ($m^3\ m^{-3}$)			
Country	Stations	n	SMOS	DisPATCh	OL	Analysed	SMOS	DisPATCh	OL	Analysed	SMOS	DisPATCh	OL	Analysed	SMOS	DisPATCh	OL	Analysed
Morocco	Sidi Rahal	104	0.64(±0.12)	0.82(±0.06)	0.74(±0.06)	0.87(±0.05)	-0.01(±0.01)	-0.01(±0.01)	0.01(±0.01)	-0.01(±0.01)	0.06(±0.01)	0.05(±0.01)	0.06(±0.01)	0.04(±0.01)	0.06(±0.01)	0.05(±0.01)	0.06(±0.01)	0.04(±0.01)
Australia	Yanco 1	104	0.69(±0.10)	0.76(±0.08)	0.63(±0.12)	0.80(±0.07)	0.06(±0.01)	0.02(±0.01)	0.08(±0.01)	0.04(±0.01)	0.08(±0.01)	0.06(±0.01)	0.09(±0.01)	0.06(±0.01)	0.06(±0.01)	0.06(±0.01)	0.05(±0.01)	0.05(±0.01)
	Yanco 2	111	0.47(±0.14)	0.69(±0.09)	0.65(±0.11)	0.79(±0.07)	-0.03(±0.01)	-0.03(±0.01)	0.03(±0.01)	-0.01(±0.01)	0.08(±0.01)	0.08(±0.01)	0.07(±0.01)	0.06(±0.01)	0.07(±0.01)	0.07(±0.01)	0.06(±0.01)	0.05(±0.01)
	Yanco 8	100	0.62(±0.12)	0.84(±0.06)	0.46(±0.16)	0.85(±0.05)	0.06(±0.01)	0.02(±0.01)	0.04(±0.01)	0.02(±0.01)	0.08(±0.01)	0.04(±0.01)	0.07(±0.01)	0.04(±0.00)	0.06(±0.01)	0.04(±0.01)	0.06(±0.01)	0.03(±0.00)
	Yanco 9	122	0.66±0.10)	0.82±0.06)	0.50±0.12)	0.84±0.05)	-0.02(±0.01)	0.01(±0.01)	-0.01(±0.01)	0.01(±0.01)	0.07(±0.01)	0.06(±0.01)	0.06(±0.01)	0.05(±0.01)	0.06(±0.01)	0.06(±0.01)	0.05(±0.01)	0.05(±0.01)
	Yanco 10	114	0.68(±0.10)	0.84(±0.05)	0.69(±0.10)	0.88(±0.04)	0.04(±0.01)	0.02(±0.01)	0.04(±0.01)	0.03(±0.01)	0.08(±0.01)	0.05(±0.01)	0.06(±0.01)	0.04(±0.00)	0.07(±0.01)	0.04(±0.01)	0.04(±0.01)	0.03(±0.00)
	Yanco 12	79	0.65(±0.13)	0.66(±0.13)	0.62(±0.14)	0.70(±0.12)	-0.04(±0.01)	-0.08(±0.01)	-0.04(±0.01)	-0.06(±0.01)	0.07(±0.01)	0.10(±0.01)	0.07(±0.01)	0.08(±0.01)	0.06(±0.01)	0.06(±0.01)	0.06(±0.01)	0.05(±0.01)
	Yanco 13	69	0.52(±0.17)	0.74(±0.11)	0.52(±0.17)	0.78(±0.09)	0.04(±0.02)	0.01(±0.01)	0.02(±0.01)	0.0(±0.01)	0.09(±0.02)	0.05(±0.01)	0.06(±0.01)	0.04(±0.01)	0.08(±0.02)	0.04(±0.01)	0.05(±0.01)	0.04(±0.01)
average			0.62	0.77	0.60	0.81	0.04	0.02	0.04	0.02	0.08	0.06	0.07	0.05	0.07	0.05	0.05	0.04

TABLE 4. GDOWN results.

Country	Site	DisPATCh	Analyzed
Morocco	Sidi Rahal	0.232	0.330
Australia	Yanco 1	0.119	0.112
	Yanco 2	0.352	0.530
	Yanco 8	0.571	0.314
	Yanco 9	0.014	0.067
	Yanco 10	0.108	0.235
	Yanco 12	-0.111	-0.066
	Yanco 13	0.282	0.220
average		0.196	0.218

TABLE 5. Temporal statistics and their 95% confidence intervals of open loop and analyzed SSM at all stations with respect to *in situ* measurement; r is the correlation coefficient, RMSE is the root mean square error, ubRMSE is the unbiased-RMSE and n is the number of comparison days. With a p-value <0.01 for all sites, statistics are significant.

			r			bias ($m^3\ m^{-3}$)			RMSE ($m^3\ m^{-3}$)			ubRMSE ($m^3\ m^{-3}$)		
Country	Station	n	OL	Analysed 25 km	Analysed 1 km	OL	Analysed 25 km	Analysed 1 km	OL	Analysed 25 km	Analysed 1 km	OL	Analysed 25 km	Analysed 1 km
Morocco	Sidi Rahal	334	0.73(±0.05)	0.66(±0.08)	0.83 (±0.03)	0.00(±0.01)	0.01(±0.01)	0.01(±0.01)	0.07(±0.00)	0.06(±0.00)	0.06(±0.00)	0.07(±0.00)	0.06(±0.00)	0.06(±0.00)
Australia	Yanco 1	247	0.60(±0.08)	0.49(±0.10)	0.64(±0.07)	0.08(±0.01)	0.06(±0.01)	0.05(±0.01)	0.10(±0.01)	0.08(±0.01)	0.08(±0.01)	0.06(±0.01)	0.05(±0.01)	0.06(±0.01)
	Yanco 2	365	0.66(±0.05)	0.30(±0.12)	0.71(±0.05)	0.03(±0.01)	0.01(±0.01)	0.03(±0.01)	0.07(±0.01)	0.07(±0.01)	0.08(±0.01)	0.06(±0.01)	0.07(±0.01)	0.08(±0.01)
	Yanco 8	360	0.40(±0.08)	0.56(±0.09)	0.66(±0.06)	0.03(±0.01)	0.04(±0.01)	0.04(±0.01)	0.08(±0.00)	0.07(±0.01)	0.07(±0.00)	0.07(±0.00)	0.05(±0.00)	0.06(±0.00)
	Yanco 9	365	0.42(±0.08)	0.52(±0.09)	0.74(±0.05)	0.02(±0.01)	0.03(±0.01)	0.02(±0.01)	0.07(±0.00)	0.06(±0.00)	0.07(±0.00)	0.07(±0.00)	0.06(±0.00)	0.06(±0.00)
	Yanco 10	348	0.47(±0.07)	0.63(±0.08)	0.70(±0.04)	0.03(±0.01)	0.04(±0.01)	0.04(±0.01)	0.08(±0.00)	0.06(±0.00)	0.07(±0.00)	0.07(±0.00)	0.05(±0.00)	0.06(±0.00)
	Yanco 12	289	0.56(±0.07)	0.37(±0.13)	0.70(±0.06)	0.05(±0.01)	0.04(±0.01)	0.05(±0.01)	0.10(±0.01)	0.08(±0.01)	0.09(±0.01)	0.07(±0.01)	0.07(±0.01)	0.07(±0.01)
	Yanco 13	241	0.35(±0.10)	0.41(±0.14)	0.61(±0.07)	0.02(±0.01)	0.02(±0.01)	0.04(±0.01)	0.08(±0.01)	0.07(±0.01)	0.07(±0.01)	0.08(±0.01)	0.06(±0.01)	0.07(±0.01)
average			0.53	0.49	0.70	0.03	0.03	0.03	0.08	0.08	0.07	0.07	0.06	0.06

LIST OF FIGURES

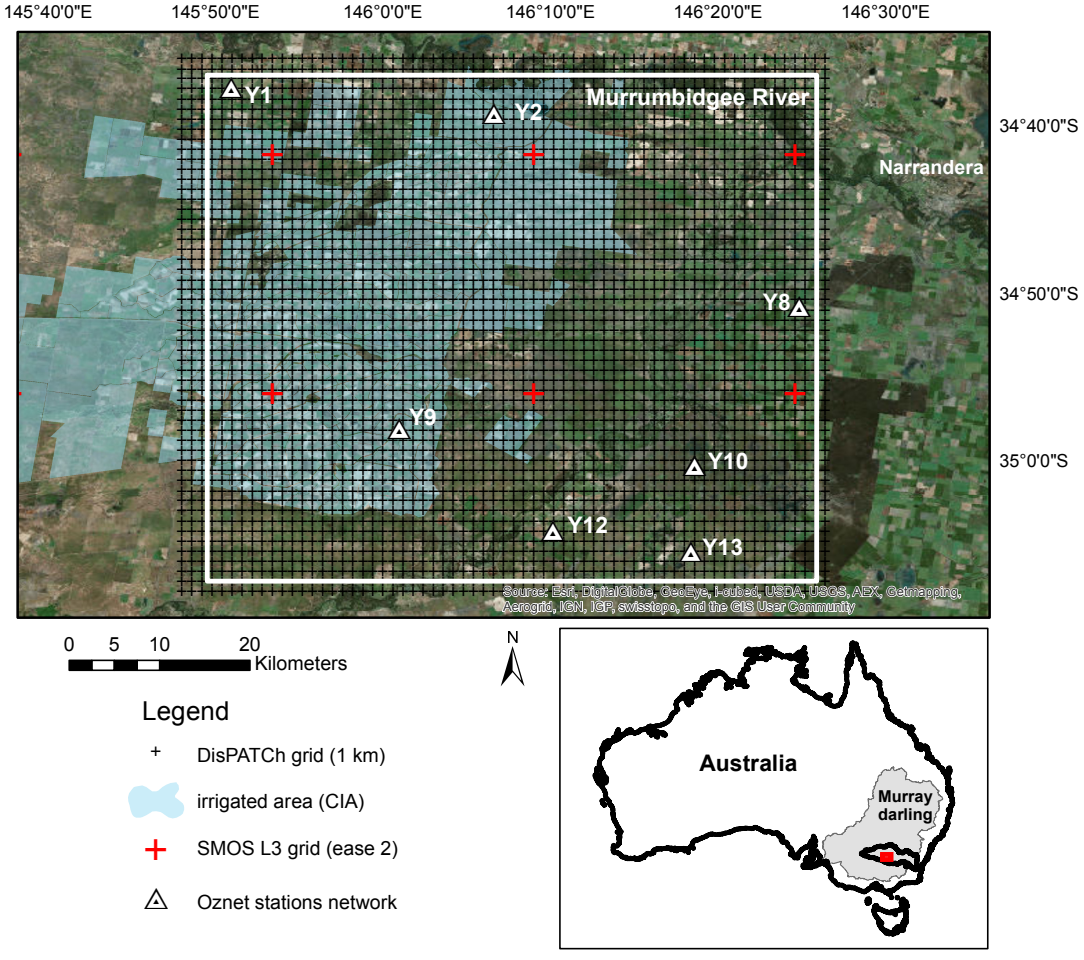

947 FIG. 1. The experimental Yanco area located in southeastern Australia showing the SMOS L3 grid corner
948 (red cross), DisPATCh grid (black cross), the selected OzNet stations, and the irrigated area.

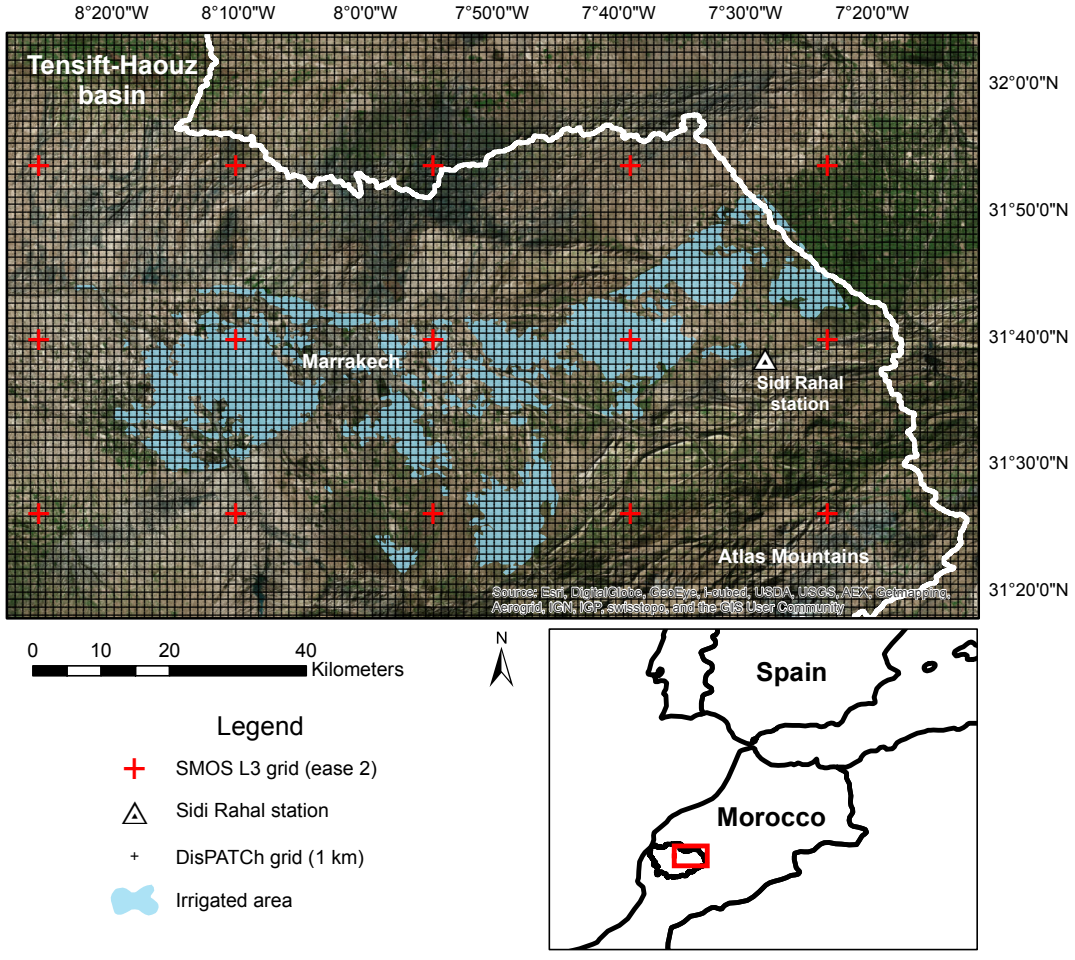

FIG. 2. The Tensift Haouz basin located in central Morocco showing the SMOS L3 grid corner (red cross), DisPATCh grid (black cross), Sidi Rahal station, and the irrigated area.

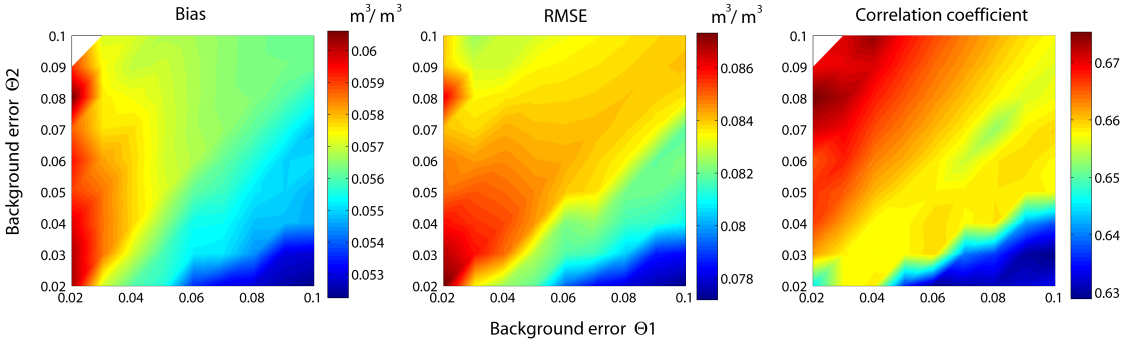

951 FIG. 3. Sensitivity analysis for background errors. An ensemble of 10 perturbations from 0.02 to 0.1 $m^3\ m^{-3}$
952 was built for both the background error terms (Θ_1 and Θ_2). The global statistics (correlation coefficient, Root
953 Mean Square Error RMSE, and mean bias) were computed based on the analyzed and in situ SSM comparison.

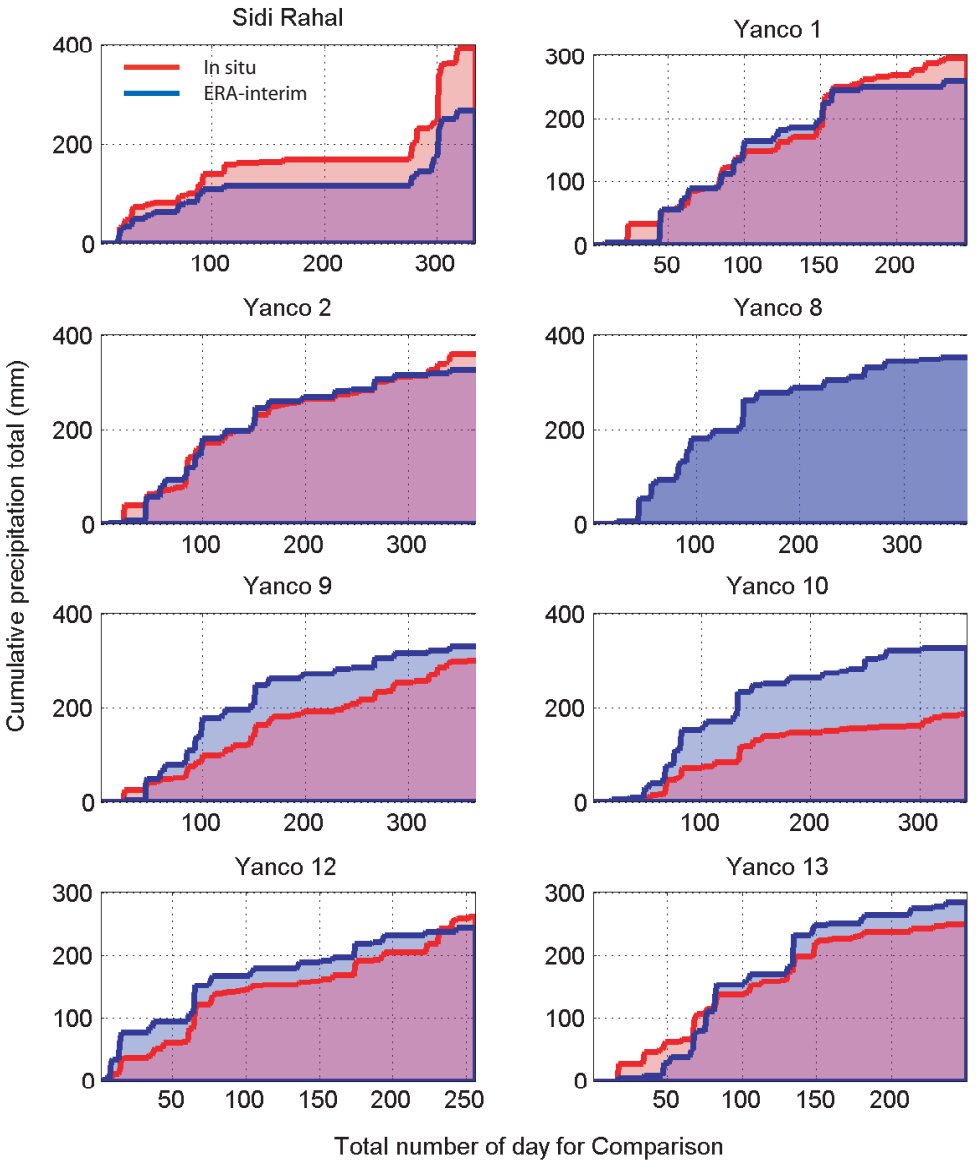

954 FIG. 4. Cumulative daily precipitation (mm) for all sites. The blue lines are the ERA-interim precipitation at
955 0.125° spatial resolution distributed by the ECMWF and the red lines are the *in situ* precipitation. Note that *in*
956 *situ* data are not available for Yanco 8.

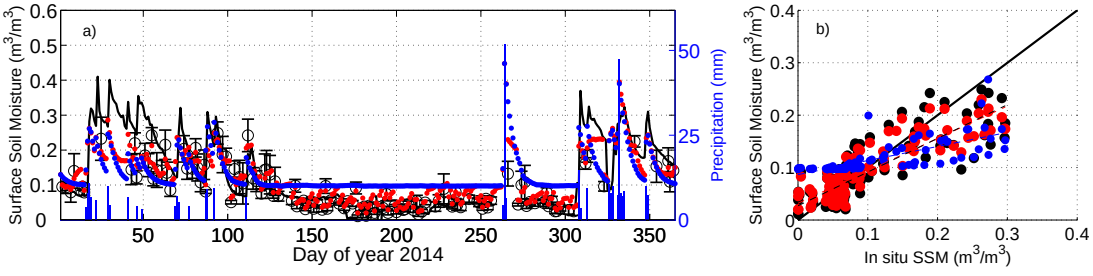

FIG. 5. (a) Time series evaluation of the DisPATCh (black circle) with the errors bars representing standard deviation of DisPATCh, open loop (blue dots), and the analyzed (red dots) SSM against *in situ* (black line) measurements and cumulative daily precipitation (blue bars) for Sidi Rahal station. (b) Scatterplot of DisPATCh (black dots), open loop (blue dots), analyzed (red dots) SSM versus *in situ* measurements.

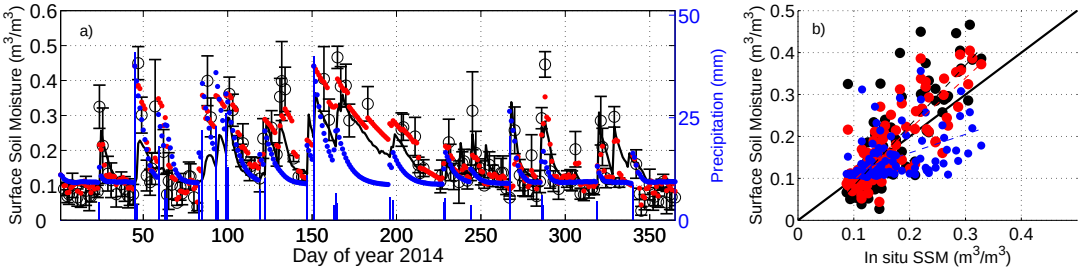

FIG. 6. As for fig. 5 but for Yanco 9 station

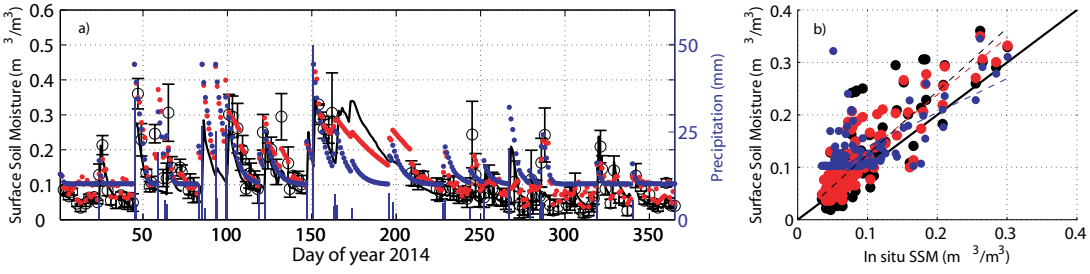

FIG. 7. As for fig. 5 but for Yanco 10 station

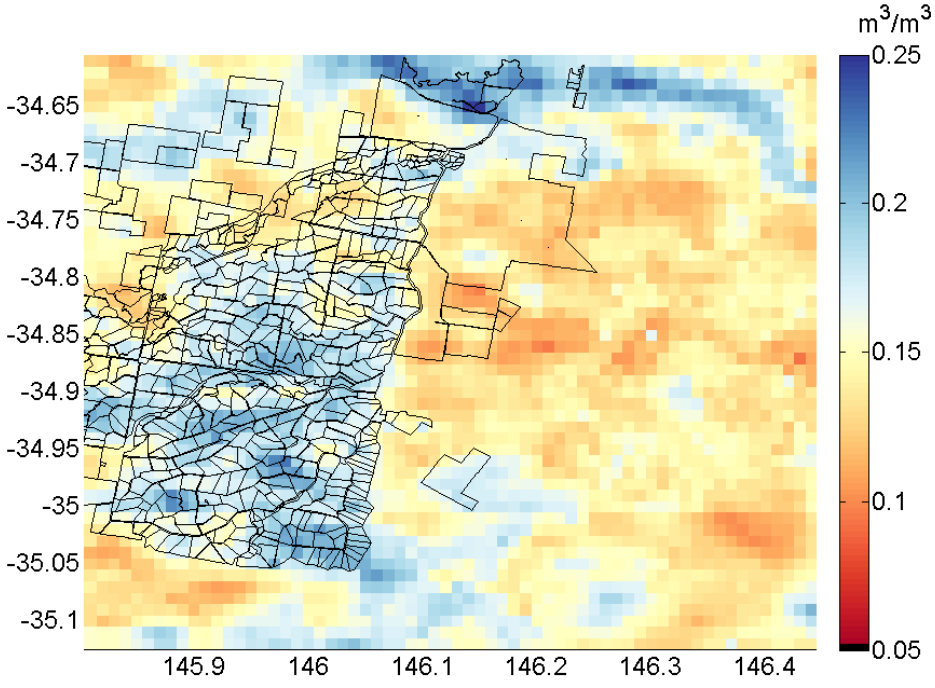

961 FIG. 8. Image of yearly (2014) average of analyzed SSM over Yanco area. Black lines represent the irrigated
962 fields.

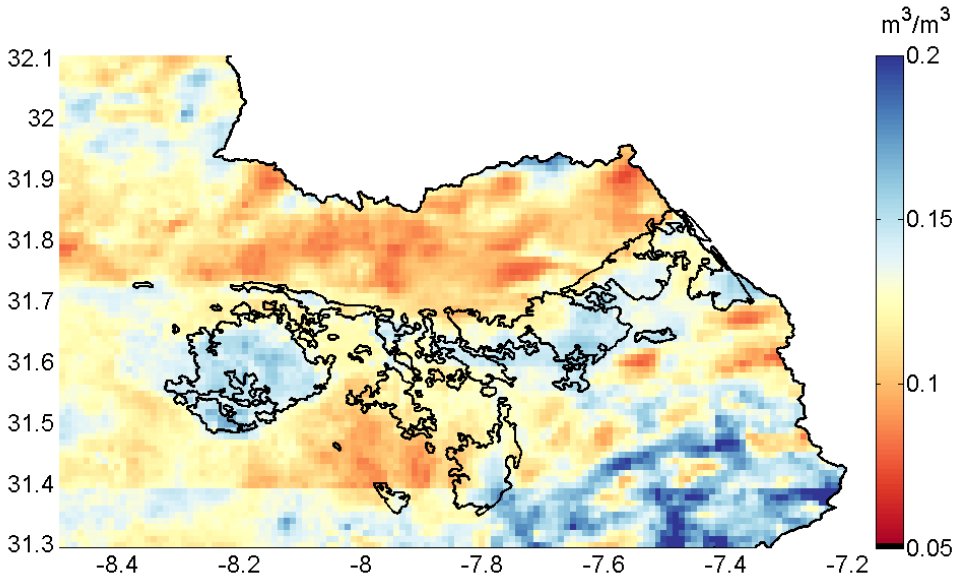

963 FIG. 9. Image of yearly (2014) average of analyzed SSM over Tensift Haouz region. Black lines represent the
964 irrigated fields.